High Dielectric Constant Semiconducting Poly(3-alkylthiophene)s from Side Chain Modification with Polar Sulfinyl and Sulfonyl Groups

Chunlai Wang,^{†,#} Zhongbo Zhang,^{†,‡,#} Sandra Pejić,[†] Ruipeng Li,[§] Masafumi Fukuto,[§] Lei Zhu,^{†,‡,*}, and Geneviève Sauvé ^{†,*}

† Department of Chemistry, Case Western Reserve University, Cleveland, Ohio 44106-7078, United States

[‡] Department of Macromolecular Science and Engineering, Case Western Reserve University,

Cleveland, Ohio 44106-7202, United States

§ National Synchrotron Light Source II, Brookhaven National Laboratory, Upon, New York
11973, United States

[#] These authors contribute equally to this work.

^{*} Corresponding authors, E-mails: https://linear.nlm.new.genera

Abstract

There is growing interest in designing and developing high dielectric constant $(\varepsilon_{\rm r})$ organic semiconductors, because they have the potential to further enhance device performance by promoting exciton dissociation, reducing bimolecular charge carrier recombination and potentially enhancing charge carrier mobility via charge-screening. In this study, a new class of semiconducting polymers with high ε_r , i.e., sulfinylated and sulfonylated poly(3-alkylthiophene)s (P3ATs), were synthesized. Because of efficient rotation of highly polar methylsulfinyl and methylsulfonyl side groups (i.e., orientational polarization), high ε_r values were achieved for these functionalized P3ATs based on an accurate capacitance measurement using a gold/semiconducting polymer/SiO₂/n-doped Si configuration. For example, the ε_r at MHz and room temperature increased from 3.75 for the regionegular poly(3-hexylthiophene) (P3HT) to 7.4 for the sulfinylated and 8.1-9.3 for sulfonylated P3AT polymers. These values are amongst the highest ε_r reported for conjugated polymers so far. Grazing-incident wide-angle X-ray diffraction results showed that these polar groups decreased the crystallinity for the polythiophene backbones, and interfered with the π - π stacking in the crystalline structure. Consequently, their optical properties, including UV-Vis absorption and fluorescence, changed in thin films. From this study, the sulfinylated polymer may be promising to provide a balance between high ε_r and preserving favorable polythiophene π - π stacking structure for device applications.

Introduction

Organic semiconductors have attracted much attention due to their potential use in electronic applications. Most research efforts have been dedicated to the optimization of semiconductors' optical, electrochemical, electrical, and structural properties. A much less investigated property of organic semiconductors is the relative permittivity or dielectric constant (ε_r) and its effect on optoelectronic properties and device performance. Organic semiconductors typically have a low ε_r , only 3 to 4, as compared to inorganic semiconductors, e.g., ε_r for Si is ~11.

High ε_r semiconductors in inorganic solar cells and lead halide perovskite solar cells all have low exciton binding energy, such as Si (15 meV), GaN (20 meV), and CH₃NH₃PbI₃ (10 meV). These excitons can easily split into free charge carriers by thermal energy k_BT (i.e., around 25 meV at room temperature) for efficient device performance.^{1,2} This could be largely attributed to their high dielectric constants at high frequencies. For example, the ε_r of lead halide perovskites at THz frequencies is about 20-28.³⁻⁶ However, excitons generated in most organic semiconductors have an exciton energy of at least 100 meV. 7-10 In order to overcome this large energy barrier to dissociate excitons, a heterojunction architecture composed of a donor and an acceptor with a proper energy level offsets must be used. Nonetheless, these energy offsets lead to a decrease in the open circuit voltage (Voc) and thereby limit the overall device performance. The dissociation probability of excitons in inorganic semiconductors such as Si is about two orders of magnitude higher than that in organic semiconductors. 11 Koster et al. predicted that exciton binding energies of organic semiconductors could be reduced to the order of k_BT, if the ε_r of organic semiconductors can be increased to $\sim 10^{12}$ This would enable a homojunction organic photovoltaics (OPVs) with a single photoactive material. Moreover, a number of authors have argued that the strength of charge screening is one of the most contributing factors to charge

dissociation in OPVs, and high ϵ_r organic semiconductors can effectively suppress charge recombination. 12-14

Increasing ε_r can be realized through enhancing various polarizations, including electronic, atomic/vibrational, and orientational/dipolar polarizations. ¹⁵ Before exploring viable approaches, it is desirable to understand the opportunities in enhancing different polarizations for polymers. First, one could utilize space charges, which include both electron/holes and ionic species. However, polarization (or conduction) of electrons and holes will not increase the capacitance and thus the ε_r of a semiconducting polymer. Interfacial polarization (or conduction) of ionic species will increase the overall capacitance (through the electric double layer, EDL) but not the genuine ε_r of a dielectric polymer. ¹⁶ Therefore, space charge polarization should not be utilized to enhance ε_r for conjugated polymers. In contrast, atomic and electronic polarizations improve ε_r at very high frequency (above THz) and could potentially reduce exciton binding energy as well as charge transfer exciton attraction. However, the ε_r enhancement from atomic and electronic polarizations has been limited between 2 to 5 due to the nature of covalent bonds for organic polymers, and there is an inverse upper-limit relationship between the bandgap and ε_r . ^{15, 17, 18}. We recently tested an idea that utilizes the keto-enol tautomeric structures in fluorescein monopotassium saltcontaining side-chain semiconducting polymers to enhance the ε_r . A relatively high ε_r of 5.5 was achieved at high frequencies, which is promising in promoting charge carrier mobility in the solid state.

Alternatively, orientational or dipolar polarization, which originates from rotation of dipolar groups, can be utilized to further enhance the ϵ_r of polymers. Dipolar polarization happens at frequencies below 10^{10} Hz, which is at the same time scale for most bimolecular recombination in organic semiconductors. An enhancement of dielectric constant and device performance could

also be achieved by blending a high-permittivity small molecule with the semiconducting polymer. 20 However, it was difficult to achieve high dielectric constants because of the macrophase separation of the small molecules at high concentrations. As a result of macrophase separation, the dielectric constant will decrease, as well as the device performance. Instead, side chain functionalization with polar groups has been shown to be a practical method for improving ε_r of organic semiconductors without deteriorating other parameters such as crystalline morphology and charge mobility. 13 de Gier et al. demonstrated that increasing ε_r of organic semiconductors with dipolar polarization can lower the Coulombic attraction between electrons and holes in the charge transfer state, if the polar groups can rotate fast enough in the solid films under the applied field. 21

Yang et al. showed that adding fluorine substituents on the backbone of a conjugated polymer (P0F) increased the ε_r from 6.6 to 7.2 for P1F with one fluorine per repeat unit, and then to 7.9 for P2F with two fluorines per repeat unit. When blended with PCBM in devices, both P1F and P2F exhibited decreased charge transfer exciton energy and improved V_{oc} when compared with P0F.²² Cho et al. demonstrated that increasing the ε_r of PIDT-DPP-alkyl (i.e., indacenodithiophene-based copolymer containing diketopyrrolopyrrole unit with alkyl chains) from 3.5 to 5.0 by incorporating highly polar nitrile groups on the side chains improved both charge carrier lifetime and device performance in a bilayer device.²³ Armin et al. synthesized a dimer and a polymer by substituting the alkyl side chain of DA (i.e., a dimer of 2-((7-(4,4-di-*n*-octyl-4H-cyclopenta[2,1-b:3,4-b']dithiophen-2-yl)benzo[c][1,2,5]thiadiazol-4-yl)methylene)malononitrile) and PCPDTBT (i.e., poly[2,6-(4,4-bis-{2-ethylhexyl}-4H-cyclopenta[2,1-b;3,4-b']dithiophene)-alt-4,7-(2,1,3-benzothiadiazole)]) with polarizable oligo(ethylene glycol) side chains.²⁴ As a result, the ε_r increased from 3.6 up to 6.1 at low frequencies. Quantum efficiency and performance of these materials in OPVs by blending with poly(3-hexylthiophene) (P3HT) were also improved.

Although some progress has been made to improve ε_r of organic semiconductors via side chain modification, the ε_r values are still limited to around 6 for conjugated polymers. Since dipolar polarization is proportional to the square of dipole moment (μ) for polar molecules, ²⁵ functional groups with a high μ can induce a larger polarization. These high μ groups include nitrate -NO₂ (~3.6 D), nitrile -CN (~3.95 D), sulfinyl -SO- (~3.96 D), and sulfonyl -SO₂- (~4.5 D) groups. Sulfonyl group has been proved to be a good candidate for enhancing ε_r of dipolar glass polymers. For example, it was demonstrated that the ε_r of poly[2-(methylsulfonyl)ethyl methacrylate] (PMSEMA) can reach 11-12 at room temperature (i.e., below its glass transition temperature, $T_g \sim 110$ °C), which is nearly 3 times that of its analogue polymer, poly(methyl methacrylate) (PMMA). ²⁶ Later, other sulfonyl-containing polymers were also synthesized, and they exhibited enhanced ε_r below the T_g due to enhanced dipolar polarization from facile rotation of sulfonyl side groups. ^{27, 28}

In this study, we intend to increase ε_r of semiconducting regioregular poly(3-alkylthiophene)s by implementing methylsulfinyl or methylsulfonyl groups at the ends of the alkyl side chains. The effect of end group functionalization on the crystalline structure of polythiophene backbones is studied by differential scanning calorimetry (DSC) and grazing-incident wide-angle X-ray diffraction (GI-WAXD). The π - π interaction and crystallinity of polythiophene backbones appears to be affected by the strong interaction among polar sulfinyl and sulfonyl end groups. As a result, the optical properties (i.e., UV-Vis absorption and fluorescence) in thin films are altered compared to neat P3HT. A new dielectric characterization method utilizing the metal/semiconducting polymer/SiO₂/n-doped Si (MPOS) sample geometry is proposed to accurately determine the ε_r of semiconducting polymers without any interference from space charge conduction. Broadband dielectric spectroscopy (BDS) results show that the ε_r values

increase from 3.75 for neat P3HT to 7.4-9.3 for functionalized P3AT polymers at 1 MHz and room temperature. Preliminary BDS results suggest that the charge carrier mobilities in these functionalized P3AT polymers are higher than that in neat P3HT. Based on these initial characterization results, we plan to study device performance for these high ε_r polymers in the future.

Experimental Section

Materials. Tetrahydrofuran (THF) was freshly distilled over CaH₂ and stored in a refrigerator before use. Anhydrous N,N-dimethylformamide (DMF) was purchased from Fisher Scientific. 2,5-Dibromo-3-hexylthiophene and 2,5-dibromo-3-(6-bromohexyl)thiophene were synthesized according to a published procedure.²⁹ *m*-Chloroperoxybenzoic acid (*m*-CPBA) was purchased from Sigma Aldrich, and was further purified according to a published procedure.³⁰ All other chemicals were purchased from either Sigma Aldrich or Fisher Scientific, and used as received.

General Characterization Methods and Instrumentation. Proton nuclear magnetic spectroscopy (1 H NMR) spectra were recorded using a 500 MHz Bruker Ascend Advance III High Definition (HD). Chemical shift for 1 H NMR was reported in parts per million (ppm) relative to tetramethylsilane, Si(CH₃)₄. Matrix-assisted laser desorption/ionization time-of-flight (MALDITOF) mass spectra (MS) were measured on a Bruker Autoflex III MALDITOF mass spectrometer, and samples were prepared from chloroform solutions using a terthiophene matrix. Molecular weight distribution (or polydispersity, PDI) was estimated from weight- (M_w) and number-average molecular weights (M_n , PDI = M_w/M_n) determined by size-exclusion chromatography (SEC) using a Tosoh HPLC-8320. The system was operated at a flow rate of 0.35 mL/min and 25 $^{\circ}$ C using

HPLC grade THF as eluent and calibrated using linear polystyrene (PS) standards. Elemental analyses (C, H, and S) were performed under optimum combustion conditions by Robertson Microlit Laboratories (Ledgewood, NJ).

UV-Vis absorption spectra were collected on a Cary 50 UV-Vis spectrometer. Fluorescence spectra were collected on a Cary Eclipse fluorescence spectrophotometer. The excitation wavelengths for solutions and films were 450 and 550 nm, respectively. All solutions were made using chloroform with 6 vol.% methanol. All films were prepared from a 10 mg/mL solution in chloroform with 6 vol.% methanol. The solution was filtered through a 0.45 µm PTFE filter, then spin-coated at 800 rpm for 60 s. All films were annealed at 150 °C for 10 min before measurement.

Thin film cyclic voltammetry (CV) measurements were performed at room temperature using an Autolab PGSTAT 302N Exo Chemie potentiostat. CV measurements were carried out using 0.1 M Bu₄NPF₆ in dry acetonitrile or DMF as the electrolyte solution and ferrocene/ferrocenium (Fc/Fc⁺) as the internal standard. The solution was purged with nitrogen for 15 min prior to the measurement. An Ag/AgNO₃ electrode was used as the reference electrode (E_{1/2} = 0.091 V vs. Fc/Fc⁺), a Pt wire was used as the counter electrode, and a polished glassy carbon (GC) electrode served as the working electrode. Films were cast from the 10 mg/mL solution in chloroform with 6 vol.% methanol, which was filtered through a 0.45 μ m PTFE filter. For CV measurement in solution, 5 mg of compound (R-P3 and P2) were fully dissolve in the electrolyte solution before measurement. All scans were performed at a scan rate of 0.1 V/s. The highest occupied molecular orbital (HOMO) energy levels were estimated from the onsets of the oxidation potential and a value of 5.1 eV vs. vacuum was used for Fc/Fc⁺, i.e., HOMO = -(E_{onset,ox} + 5.1) eV.

Thermal gravimetric analysis (TGA) was performed on a TA instrument Q500 thermogravimetric analyzer. Weight loss was recorded by heating the sample from 25 to 800 °C at a heating scan rate of 20 °C/min. DSC was performed on a TA Instruments Q2000 differential scanning calorimeter with a scanning rate of 10 °C/min up to 300 °C.

Dielectric constants of semiconducting polymers were characterized using a gold/semiconducting polymer/SiO₂/*n*-doped Si configuration. Polymer films were cast on the SiO₂ surface from different solutions with a concentration of 20 mg/mL; P3HT in *o*-dichlorobenzene, P1 in 1:1 (vol./vol.) dichloromethane and DMF, and P2 and P3 in DMF. With an optimized solvent evaporation process, the polymer film thickness had a standard deviation of 10-15%. Gold electrodes of 2.4 mm in diameter and ~10 nm in thickness were evaporated on the top surface of the polymer films for broadband dielectric spectroscopy (BDS) characterization. Capacitance measurements were performed on a Novocontrol Concept 80 Broadband Dielectric Spectrometer with frequency from 1 to 10⁶ Hz and temperature from -50 to 75 °C at 1.0 V_{rms} (i.e., root-mean square voltage).

Tapping-mode atomic force microscopy (AFM) was performed on polymer films using a Bruker Veeco Digital Instrument 3100 microscope and a Nanoscope controller. AFM images were analyzed by Windows Application for Data Processing in Scanning Probe Microscopy (WSxM 5.0) Develop 8.0.

GI-WAXD measurements were performed using the 11-BM Complex Materials Scattering (CMS) beamline at the National Synchrotron Light Source II (NSLS-II), Brookhaven National Laboratory. The monochromatized X-ray wavelength was $\lambda = 0.0918$ nm. An in-vacuum CCD detector (Photonic Science) was used to collect GI-WAXD patterns. The polymer films were illuminated by the collimated X-ray beam at an incidence angle of about 0.1° . The distance

between the sample and the detector was 222.2 mm, which was calibrated using silver behenate with the first-order reflection at a scattering vector of q = 1.076 nm⁻¹. The data acquisition time for each GI-WAXD pattern was 10 s. Polar (Stony Brook Technology and Applied Research, Inc., Stony Brook, NY) software was used for data analysis.

Monomer and Polymer Syntheses

Sodium 4-(methylsulfonyl)butanoate (1). Ethyl 4-bromobutanoate (15 mL, 0.1 mol), 50 mL sodium thiomethoxide solution (20 wt.%, 0.12 mol), and 90 mL DMF were added into a 500 mL one-neck round-bottom flask and the mixture was stirred at 25 °C for 48 h. The reaction was quenched with 60 mL cold water and then was extracted 3 times with diethyl ether, washed one time with brine, dried with anhydrous magnesium sulfate, filtered through filter paper, and evaporated to obtain a colorless oil product, ethyl 4-(methylthio)butanoate, 5.1g (31.4mmol, 31% isolated yield). ¹H NMR (500 MHz, CDCl₃, δ): 4.14 (q, J = 7.1Hz, -COOCH₂-, 2H), 2.54 (t, J = 7.2 Hz. $-SCH_2$ -, 2H) 2.43 (dd, J = 7.9 Hz, $-OOCCH_2$ -, 2H), 2.10 (s, $-SCH_3$, 3H), 1.93 (p, J = 7.3 Hz, $-SCH_2CH_2$, 2H), 1.26 (t, J = 7.1 Hz, $-OOCCH_2CH_3$, 3H) (Figure S1). (methylthio)butanoate (2 g, 12.33 mmol) and 2.5 mL ethanol were added into 25 mL 2M NaOH solution and stirred at 40 °C for 12 h. The reaction was cooled down using an ice bath and then neutralized with hydrochloric acid. The mixture was then extracted 3 times with diethyl ether, washed with brine, dried with anhydrous magnesium sulfate, filtered through filter paper, and evaporated to obtain a colorless oil product, 4-(methylthio)butanoic acid, 1.37 g (10.2 mmol, 83% isolated yield). ¹H NMR (500 MHz, CDCl₃, δ): 2.57 (t, J = 7.1 Hz, -SC H_2 -, 2H), 2.52 (t, J = 7.3 Hz, HOOCC H_2 -, 2H), 2.11 (s, -SC H_3 , 3H), 1.95 (p, J = 7.2 Hz, -SC H_2 C H_2 -, 2H) (Figure S2). 4(Methylthio)butanoic acid (1.37 g, 10.2 mmol) and 10 mL acetic acid were added into 50 mL one-neck round-bottom flask and 1.2 mL hydroperoxide solution (30 wt.%, 10 mmol) were added dropwise into the reaction and stir at 25 °C for 1 h. Then, 2.4 mL hydroperoxide solution (30 wt.%, 20 mmol) were added dropwise into the reaction and stir at 60 °C for 4h. The reaction was quenched by adding sodium metabisulfite (0.76 g, 4 mmol), and acetic acid and water were evaporated to obtain a white solid, sodium 4-(methylsulfonyl)butanoate (1), 1.2 g, (6.4 mmol, 64% isolated yield). ¹H NMR (500 MHz, CDCl₃, δ): 3.12-3.18 (m, -SO₂CH₂-, 2H), 2.95 (s, -SO₂CH₃, 3H), 2.37 (dd, J = 9.37 Hz, -OOCCH₂-, 2H), 2.01-2.10 (m, -SO₂CH₂CH₂-, 2H) (Figure S3).

Regioregular Poly(3-hexylthiophene) (P3HT). P3HT was synthesized by the Grignard metathesis (or GRIM) method,³¹ 0.5 g (33% yield). ¹H NMR (500 MHz, CDCl₃, δ): 6.96 (s, =CH-, 1H), 2.68-2.85 (m, -ArCH₂CH₂CH₂-, 2H), 1.61-1.75 (m, -ArCH₂CH₂CH₂-, 2H), 1.37-1.74 (m, -ArCH₂CH₂CH₂-, 2H), 1.27-1.36 (m, -CH₂CH₂CH₃, 4H), 0.85-0.94 (m, -CH₃, 3H) (Figure S4). SEC: M_n = 9900 g mol⁻¹ and PDI = 1.30.

Regioregular Poly[3-(6-bromohexyl) thiophene] (P-BrHT). P-BrHT was synthesized according to the literature procedure, $^{29, 32}$ 0.58 g (46.4% yield). 1 H NMR (500 MHz, CDCl₃, δ): 6.96 (s, =CH-, 1H), 3.41 (t, J=6.4Hz, BrCH₂CH₂-, 2H), 2.72-2.87 (m, -ArCH₂CH₂CH₂-, 2H), 1.87 (t, J=6.5Hz, BrCH₂CH₂-, 2H), 1.63-1.78 (m, -ArCH₂CH₂CH₂-, 2H), 1.39-1.55 (m, BrCH₂CH₂CH₂-, 4H) (Figure S5). SEC: M_n = 10800 g mol⁻¹ and PDI = 1.28. MALDI-TOF MS for P-BrHT is shown in Figure S10.

Poly[3-(6-methylthiolhexyl)thiophene] (P-MeST). P-BrHT (0.2 g) and sodium thiomethoxide (0.23 g, 3.3 mmol) were added to a 50 mL one-neck round-bottom flask, which was vacuumed and purged with dry N₂ three times. Dry THF (16 mL) and anhydrous DMF (18 mL) were added to the flask using syringes and stirred at 50 °C under N₂ atmosphere for 36 h. The

reaction was cooled down to room temperature and poured into methanol to precipitate the product. The precipitate was collected into a Soxhlet thimble and extracted with methanol and chloroform. The product was collected from the chloroform fraction. After evaporating chloroform, the product was obtained as a dark green solid film (0.15 g, 86% isolated yield). ¹H NMR (500 MHz, CDCl₃, δ): 6.96 (s, =C*H*-, 1H), 2.71-2.85 (m, -ArC*H*₂CH₂CH₂-, 2H), 2.43-2.53 (m, -SC*H*₂-, 2H), 2.07 (s, -SC*H*₃, 3H), 1.68-1.76 (m, -ArCH₂CH₂CH₂-, 2H), 1.57-1.66 (m, -SCH₂CH₂-, 2H), 1.38-1.51 (m, -SCH₂CH₂CH₂-, 4H) (Figure S6).

Poly[3-(6-methylsulfinylhexyl)thiophene] (P1).³³ P-MeST (0.15 g) was dissolved in 20 mL of dichloromethane in a 50 mL one-neck round bottom flask and stirred at 0 °C. Purified *m*-CPBA (0.13 g, 0.7 mmol) was dissolved in 2 mL dichloromethane and the solution was added dropwise into the flask in 10 min. After stirring at 0 °C for 30 min, the reaction was poured into diethyl ether to precipitate the product. The precipitate was collected into a Soxhlet thimble and extracted with diethyl ether and chloroform. The product was collected from the chloroform fraction. After evaporating chloroform, P1 was obtained as a dark green solid film (70 mg, 51% isolated yield). ¹H NMR (500 MHz, CDCl₃, δ): 6.95 (s, =CH-, 1H), 2.80 (t, -ArCH₂-, 2H), 2.59-2.74 (m, -SOCH₂-, 2H), 2.53 (s, -SOCH₃, 3H), 1.73-1.83 (m, -ArCH₂CH₂-, 2H), 1.64-1.74 (m, -SOCH₂-CH₂-, 2H), 1.39-1.56 (m, -SOCH₂CH₂CH₂CH₂-, 4H) (Figure S7). Elemental analysis: Calcd. for (C₁₁H₁₆OS₂)_n: C: 56.53%; H:6.91%; S:27.44%. Found: C: 56.45%; H: 7.09%; S: 25.93%. MALDI-TOF MS for P1 is shown in Figure S11.

Poly[3-(6-methylsulfonylhexyl)thiophene] (P2). P-MeST (0.15 g) was dissolved in 20 mL of dichloromethane in a 50 mL one-neck round bottom flask and stirred at 25 °C. Purified *m*-CPBA (0.27 g, 1.5 mmol) was dissolved in 2 mL dichloromethane and the solution was added dropwise into the flask in 10 min. After stirring at 25 °C for 5 min, the reaction was poured into

diethyl ether to precipitate the product. The precipitate was collected into a Soxhlet thimble and extracted with diethyl ether and chloroform. The product was collected from the chloroform fraction. After evaporating chloroform, P2 was obtained as a dark green solid (80 mg, 46% isolated yield). ¹H NMR (500 MHz, CDCl₃, δ): 6.96 (s, =CH-, 1H), 2.95-3.04 (m, -SO₂CH₂-, 2H), 2.87 (s, -SO₂CH₃, 3H), 2.70-2.83 (m, -ArCH₂-, 2H), 1.79-1.92 (m, -SO₂CH₂CH₂-, 2H), 1.64-1.77 (m, -ArCH₂CH₂-, 2H), 1.38-1.58 (m, -SO₂CH₂CH₂CH₂CH₂-, 4H) (Figure S8). Elemental analysis: Calcd. for (C₁₁H₁₆O₂S₂)_n: C 53.46%; H 6.55%; S 25.95%. Found: C 53.24%, H 6.21%, S 24.54%. MALDI-TOF MS for P2 is shown in Figure S12.

Poly 3-[6-(3-methylsulfonylpropylcarbonyloxy)hexyl]thiophene (P3). P-BrHT (0.15 g) and 1 (0.4 g, 2 mmol) were added into a 50 mL one-neck round-bottom flask which was vacuumed and purged with N₂ three times. Dry THF (8 mL) and anhydrous DMF (18 mL) were added to the flask using syringes and stirred at 50 °C under N₂ for 72 h. The reaction was cooled to room temperature and poured into methanol to precipitate the product. The precipitate was collected into a Soxhlet thimble and extracted with methanol and chloroform. The product was collected into the chloroform fraction. After evaporating chloroform, P3 was obtained as a brown solid film (0.18 g, 89% isolated yield). ¹H NMR (500 MHz, CDCl₃, δ): 6.96 (s, =CH-, 1H) 4.07 (t, J=6.5Hz, -COOCH₂-, 2H), 3.03-3.13 (m, -SO₂CH₂-, 2H), 2.87 (s, -SO₂CH₃, 3H), 2.71-2.84 (m, -ArCH₂-2H), 2.49 (t, -OOCCH₂-, J=6.9Hz, 2H), 2.07-2.17 (m, -SO₂CH₂CH₂-, 2H), 1.56-1.65 (m, -ArCH₂CH₂-, 2H), 1.65-1.75 (m, -COOCH₂CH₂-, 2H), 1.34-1.50 (m, -COOCH₂CH₂CH₂-, 4H) (Figure S9). Elemental analysis: Calcd. for (C₁₅H₂₂O₄S₂)_n: C 54.51%; H 6.74 %; S 19.41%. Found: C 54.72%, H 6.51%, S 19.69%. MALDI-TOF MS for P3 is shown in Figure S13.

(a)
$$P$$
-BrHT P -MeST P -MeS

Scheme 1. (a) Synthesis of poly[3-(6-methylsulfinylhexyl)thiophene] (P1) and poly[3-(6-methylsulfonylhexyl)thiophene] (P2). (b) Synthesis of sodium 4-(methylsulfonyl)butanoate (1). (c) Synthesis of poly 3-[6-(3-methylsulfonylpropylcarbonyloxy)hexyl]thiophene (P3).

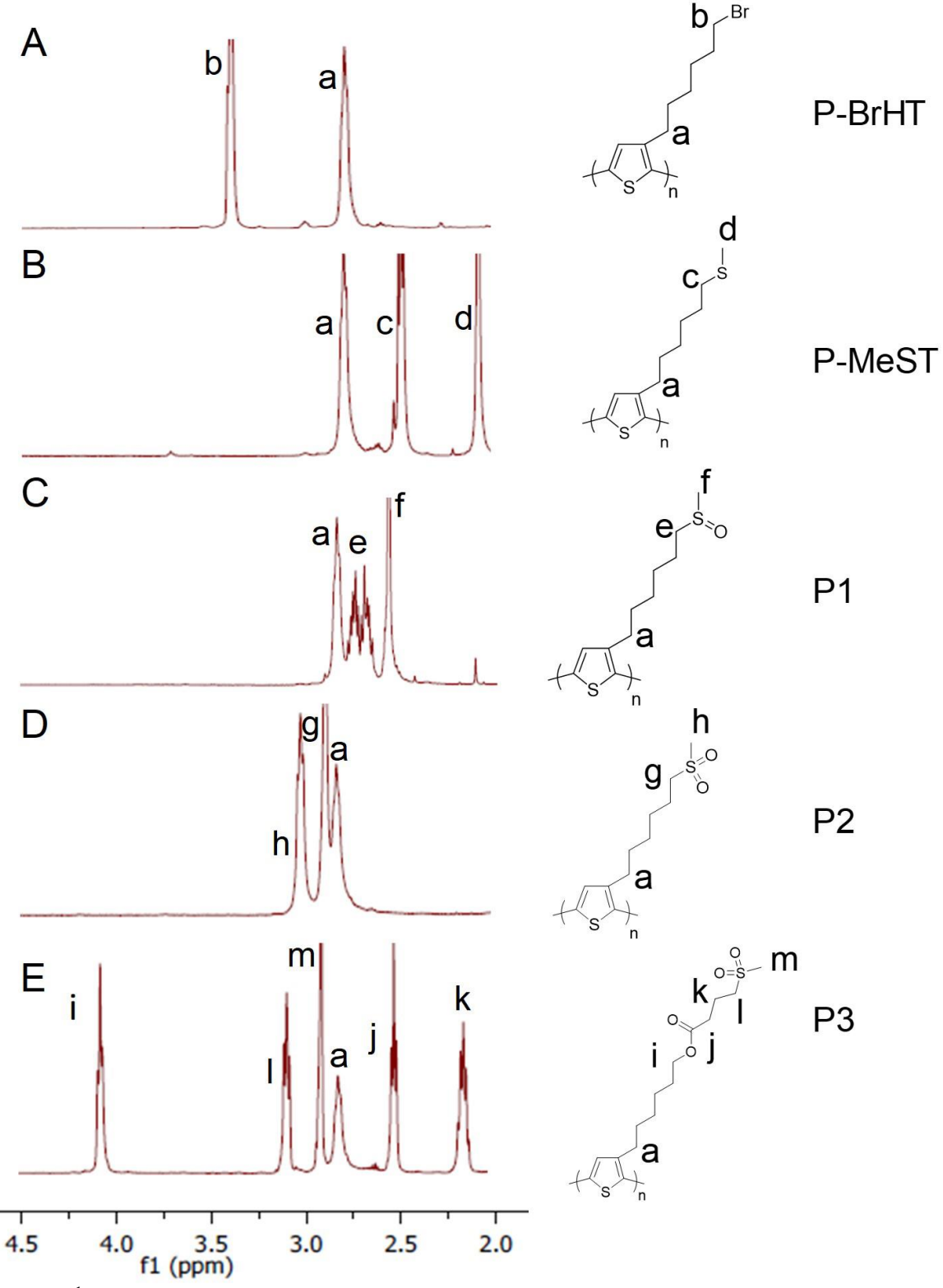


Figure 1. ¹H NMR of spectra of various functionalized P3AT polymers in CDCl₃: (A) P-BrHT, (B) P-MeST, (C) P1, (D) P2, and (E) P3.

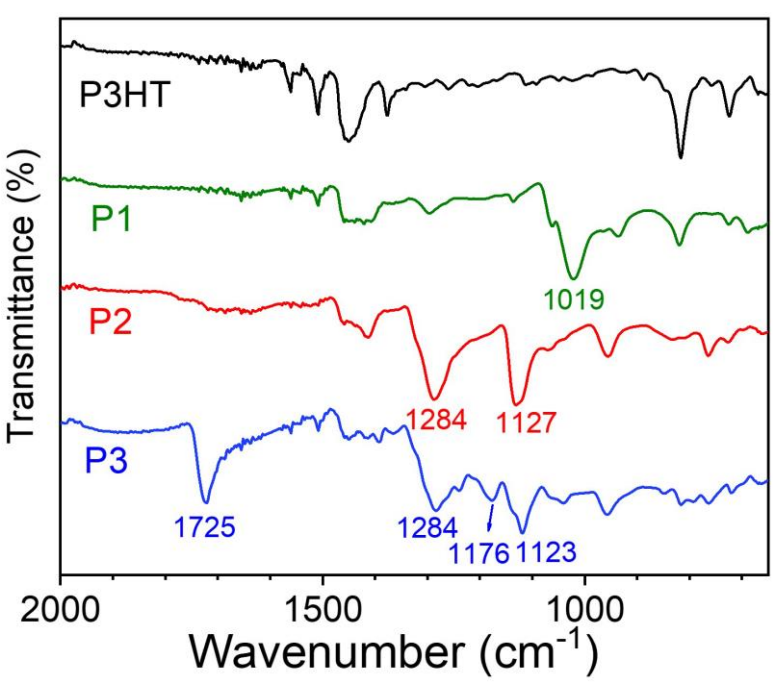


Figure 2. Transmission FTIR spectra of P3HT, P1, P2, and P3, respectively.

Result and Discussion

Monomer and Polymer Syntheses. Synthesis routes for functionalized P3AT polymers are shown in Scheme 1. The precursor poly[3-(6-bromohexyl)thiophene] (P-BrHT) was synthesized using the published method by McCullough.²⁹ The structure of P-BrHT was confirmed by MALDI-TOF (Figure S10). The measured repeat unit mass for P-BrHT (245.03 m/z) is close to the calculated mass of repeat unit (245.01 m/z). The average molar molecular weight of P-BrHT was estimated by SEC at 10800 g/mol, about 44 repeat units. The bromines in P-BrHT were substituted with methylthiolether groups by reaction with sodium thiomethoxide in DMF (P-MeST in Scheme 1a).³³ The ¹H NMR spectra of P-BrHT and P-MeST are shown in Figures 1A and 1B, respectively. Peak b at 3.5 ppm was assigned to the CH₂ next to the bromine at the chain end of P-BrHT. In P-MeST, the methylene protons next to the bromine (peak b) completely disappeared, indicating that the S_N2 reaction was quantitative. About 1.1 equivalents of *m*-CPBA were used to react with P-MeST at 0 °C for 40 min to obtain P1. The ¹H NMR

spectrum in Figure S7 indicates that the oxidizations from P-MeST to P1 was selective and quantitative, with no obvious oxidization of the sulfinyl group and thiophenic sulfur was observed. The successful oxidization of the -SCH₃ groups in P-MeST was also confirmed by FTIR, as shown in Figure 2. In P1, the peak at 1019 cm⁻¹ was attributed to the S=O stretching in the sulfinyl group. MALDI-TOF in Figure S11 also confirms the repeat-unit mass of P1 (observed 229.42 m/z and calculated 230.08 m/z).

P2 was synthesized by using 2.5 equivalents of *m*-CPBA as oxidizer under 25 °C, and ¹H NMR indicated that all -SCH₃ groups in P-MeST were oxidized into methylsulfonyl groups (Figure S8A). The successful oxidization was further confirmed by FTIR, as shown in Figure 2. The peak at 1019 cm⁻¹ disappeared and peaks at 1284 and 1127 cm⁻¹ appeared, due to the asymmetric and symmetric O=S=O stretching, respectively. MALDI-TOF in Figure S12 also confirms the repeat-unit mass of P2 (observed 246.01 m/z and calculated 246.07 m/z). Due to solubility issues, we could not measure M_n for P1 and P2 by SEC.

Nucleophile 1 was obtained by a three-step reaction, as shown in Scheme 1b, with an overall yield of 17%. Nucleophile 1 was then reacted with P-BrHT to obtain P3 with side chains containing one sulfonyl and one ester groups, separated by three CH₂ groups (see Scheme 1C). The ¹H NMR spectra of P3 (Figure 1E) shows that peak b completely disappeared, indicating a quantitative S_N2 reaction. FTIR confirmed the presence of ester and sulfonyl groups in P3: the absorption bands at 1725 and 1176 cm⁻¹ corresponded to the C=O and C-O stretching in the ester group, respectively, and the absorption bands at 1284 and 1123 cm⁻¹ corresponded to the asymmetric and symmetric O=S=O stretching, respectively. MALDI-TOF in Figure S13 also confirms the repeat-unit mass of P3 (observed 330.50 m/z and calculated 331.11 m/z).

The solubility of these functionalized P3AT polymers was strongly affected by the polar groups at the side-chain ends: P1, P2 and P3 were more soluble in polar solvents and less soluble in nonpolar solvents, as compared to P3HT. P3HT was readily soluble in chlorinated solvents such as chloroform and dichlorobenzene, and insoluble in polar solvents such as DMF and dimethyl sulfoxide (DMSO). On the other hand, P1, P2 and P3 were insoluble in dichlorobenzene, but soluble in DMF and DMSO (<25 mg/mL). P1 and P3 had a high solubility, i.e., >30 mg/mL, in chloroform, whereas P2 had a low solubility of <5 mg/mL in chloroform. We found that P1, P2, and P3 all had good solubilities of >30 mg/mL in chloroform with 6 vol.% of methanol (see light scattering results in Figure S14). Sulfonyl groups are polar and tend to aggregate in nonpolar solvents, such as chloroform or dichlorobenzene. The addition of some polar solvents, such as methanol or ethanol, could break the aggregation and increase the solubility of P1-P3 in a low polarity solvent.

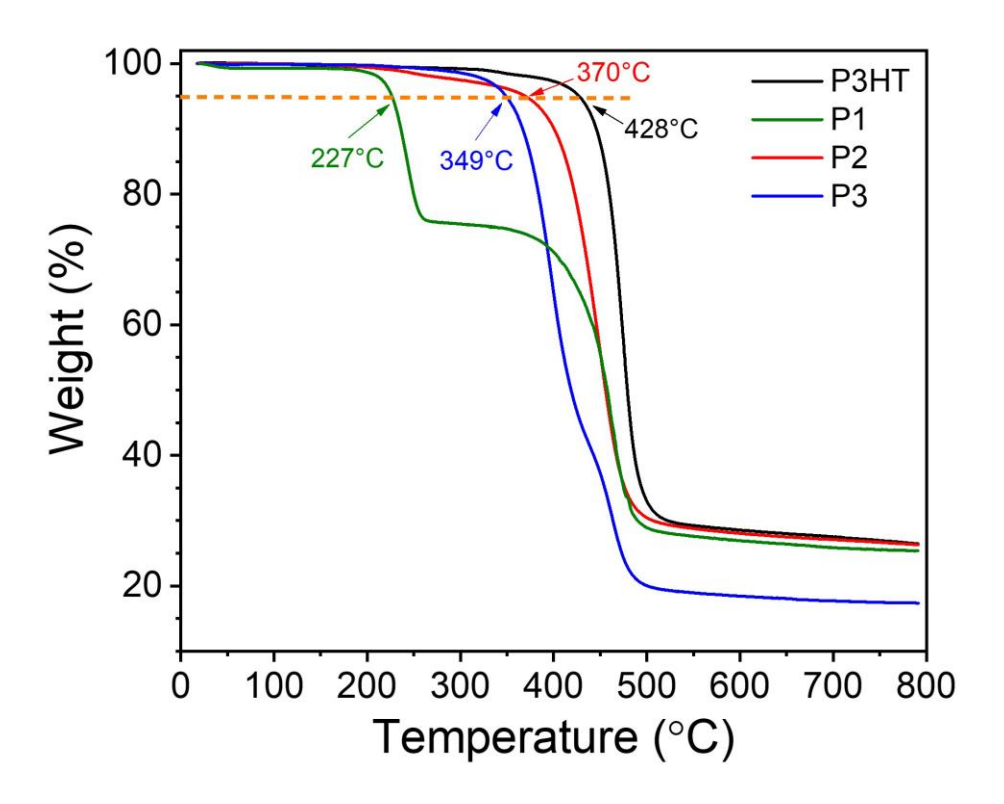


Figure 3. TGA curves for P3HT, P1, P2, and P3. The heating rate was 20 °C/min under a dry nitrogen flow.

Thermal Properties. TGA results are shown in Figure 3. For P3HT, only one thermal degradation process was observed with a 5% weight loss at 428 °C, which is close to the reported value of 440 °C.³⁴ P1 showed a 24% weight loss from 227 to 250 °C, corresponding to the weight loss of the methylsulfinyl group. P3 showed ~50% weight loss from 349 to 417 °C, due to the loss of methylsulfonyl and ester groups. While side chain functionalization decreased the polymer stability relative to neat P3HT, all polymers were stable below 200 °C, which should be sufficient for most device fabrication conditions.

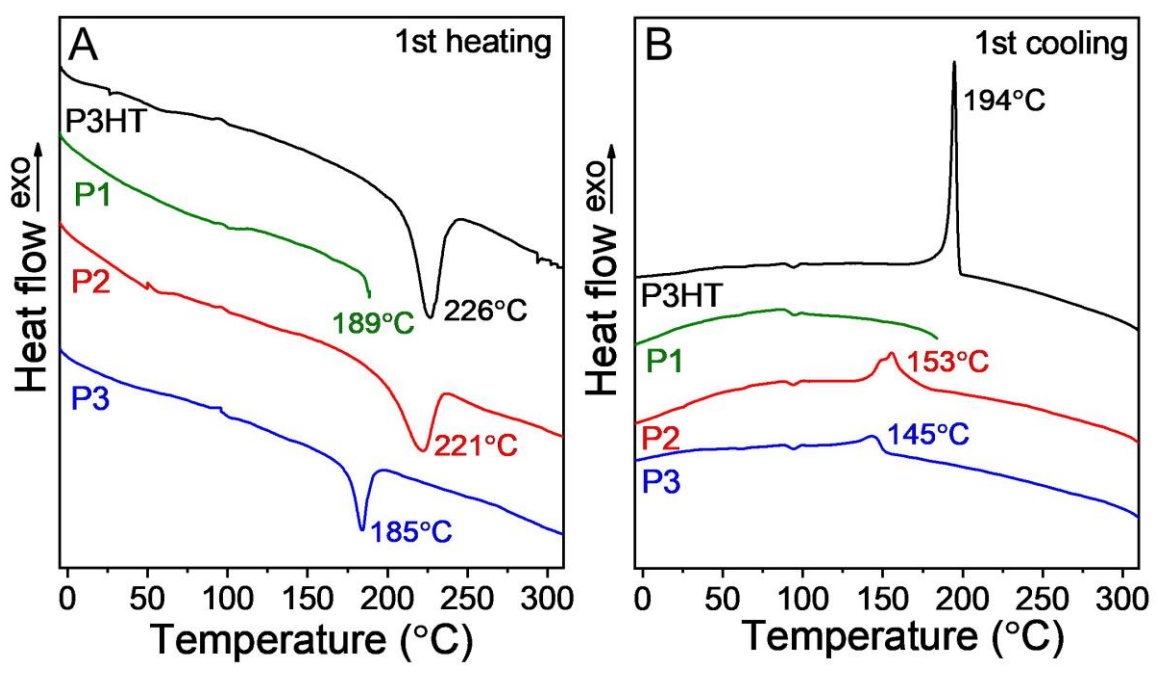


Figure 4. DSC curves for P3HT, P1, P2, and P3 during (A) the first heating and (B) the first cooling processes. The heating and cooling rates were 10 °C/min. DSC samples were prepared by drop casting polymers from chloroform with 6 vol.% methanol in DSC pans.

These functionalized P3AT polymers were crystalline, and their melting and crystallization behavior were studied by DSC (Figure 4). All solution-cast samples were heated from -10 to

320 °C at a ramp rate of 10 °C/min, except for P1, which was heated from -10 to 190 °C to avoid thermal degradation. For P3HT, the observed melting temperature (T_m) at 226 °C and the crystallization temperature (T_c) at 194 °C were close to reported values. P1 started to melt around 189 °C at the end of the first heating cycle, before significant thermal degradation happened. Both P2 and P3 had lower T_m and T_c than P3HT. The heats of fusion for all polymers during the first heating process were calculated except for P1, which did not exhibit a full melting peak in the DSC curve. P3HT had a heat of fusion (ΔH_f) of 20.0 J/g and the crystallinity was calculated to be 41% by using the heat of fusion (ΔH_f) of 49 J/g for 100% crystalline P3HT. Their crystallinities are not calculated because no ΔH_f 0 values are available for P1-P3. Glass transitions for P1-P3 could not be clearly identified from DSC. We speculate that this could be possibly attributed to the strongly interacting P1-P3 with a small entropy change before and after the glass transition.

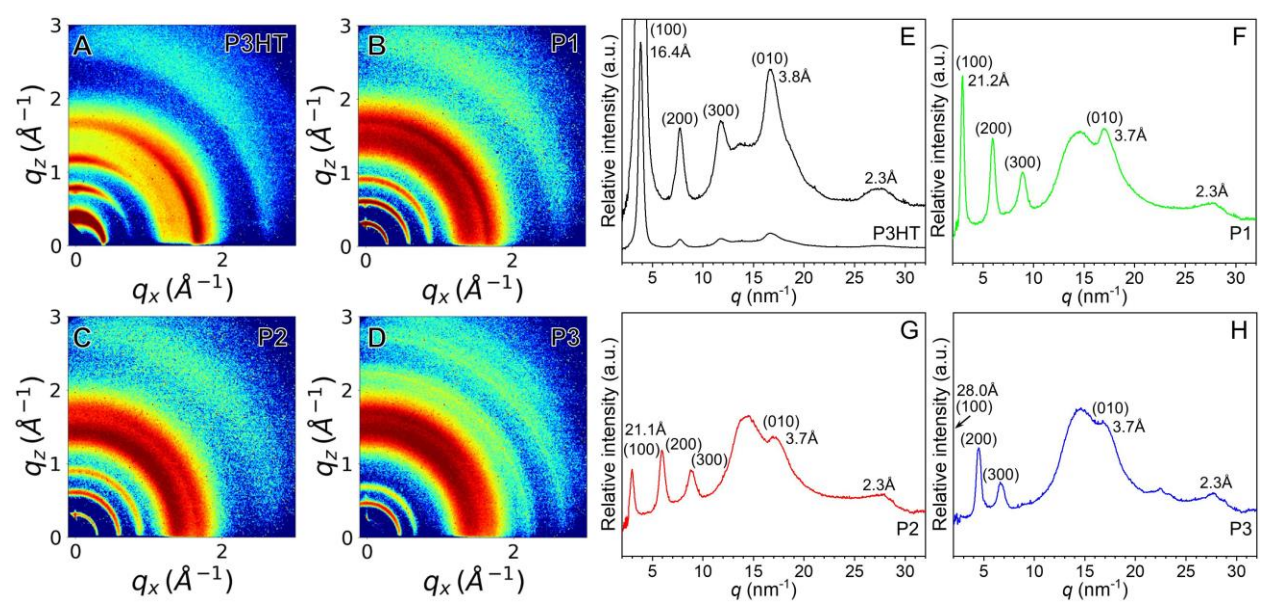


Figure 5. 2D GI-WAXD patterns of (A) P3HT, (B) P1, (C) P2, and (D) P3 measured for solution-cast thin films (~1 μm thick) and (b) 1D WAXD profiles of (E) P3HT, (F) P1, (G) P2, and (H) P3 integrated from the corresponding GI-WAXD patterns in (A-D).

GI-WAXD. The effects of the sulfinyl and sulfonyl functional groups on the crystalline structure and π - π stacking in solution-cast films were investigated by GI-WAXD. As shown in Figure 5A, the GI-WAXD pattern of P3HT exhibited well-oriented (100) reflection in the vertical direction and (010) reflection (i.e., the π - π stacking) in the horizontal direction, indicating the monoclinic crystalline structure with horizontal lamellar stacking and edge-on P3HT orientation. From the integrated 1D profile in Figure 5E, the crystallinity for P3HT was estimated to be 80%; however, this estimation is inaccurate, because the solution-cast P3HT film exhibited an obvious crystal orientation in Figure 5A. For P1-P3 films, no crystal orientation was observed in the 2D GI-WAXD patterns (Figures 5B-D); therefore, the crystallinity estimation from the 1D GI-WAXD profiles should be more accurate. It is possible that the crystallite sizes were so small that a random crystal orientation existed in solution-cast P1-P3 films. From the 1D profiles (Figures 5F-H), crystallinities were estimated to be 36% for P1, 31% for P2, and 32.5% for P3, respectively. Note that the π - π stacking in P1-P3 became much poorer compared to P3HT, as reflected by weak (010) reflections around 17.0 nm⁻¹.

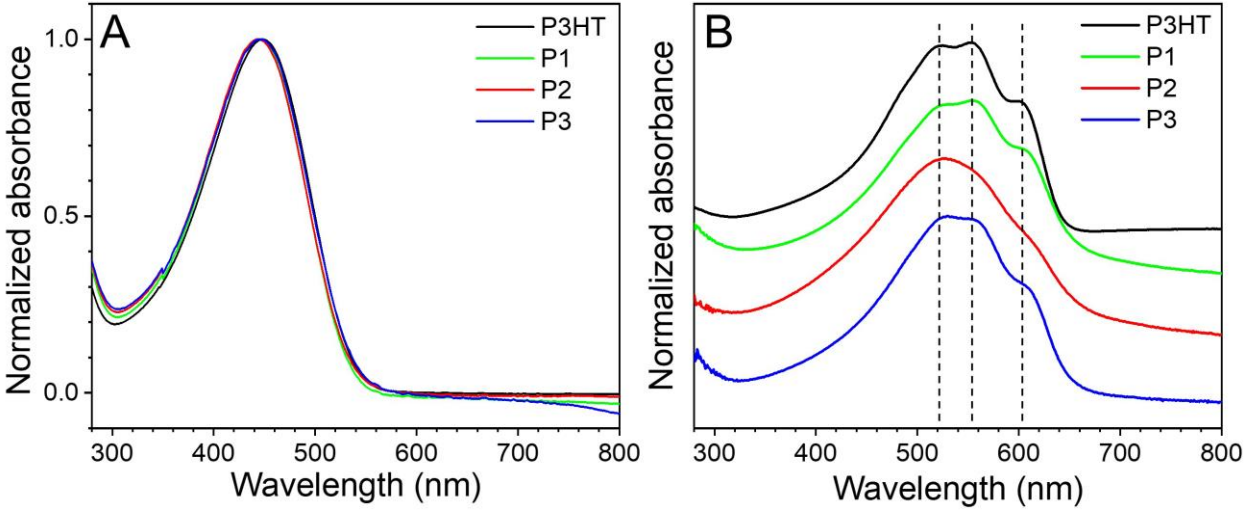


Figure 6. UV-Vis absorption spectra of P3HT, P1, P2, and P3 in (A) solution and (B) spin-coated thin films (around 65 nm), respectively. All absorbance intensities are normalized. In (B), curves are offset for clarity.

Table 1. Physical and Optical Properties of P3HT and Functionalized P1-P3.

	Solution			Film					
Polymer	M _n (kDa)	PDI	λ_{max} (nm)	λ _{onset} (nm)	λ_{max} (nm)	λ_{onset} (nm)	E _{g,opt} (eV)	HOMO (eV)	LUMO (eV)
РЗНТ	9.9	1.3	450	534	525, 552, 601	643	1.93	-5.15	-3.22
P1	11.3	1.28	445	531	530, 554, 602	674	1.84	-5.24	-3.40
P2	12.1	1.28	444	531	528	658	1.88	-5.22	-3.34
Р3	16.3	1.28	446	535	530, 554, 604	686	1.81	-5.21	-3.40

Polymer films (around 65 nm) were spin-coated from chloroform with 6 vol.% methanol. HOMO energy levels were estimated from the onset of the oxidation waves using the value of -5.1 eV for Fc/Fc^+ . Optical band gap ($E_{g,opt}$) values were estimated from the thin film UV-Vis absorbance. Lowest unoccupied molecular orbital (LUMO) values were calculated by adding values of $E_{g,opt}$ to the HOMO levels. M_n of P1, P2 and P3 were calculated by assuming the degrees of polymerization (DPs) of P1, P2 and P3 were the same as that of the precursor P-BrHT (DP \sim 44).

Optical Properties. UV-Vis absorption spectra of functionalized P3ATs were measured in both solution (Figure 6A) and spin-coated films (Figure 6B). Results are summarized in Table 1. All polymers had similar absorption spectra in solution, indicating that the functional groups did not electronically couple with the polythiophene backbone. Upon film formation, all absorption spectra red-shifted, indicating that the polythiophene backbones planarized upon film formation. The spectrum of the P3HT film showed three obvious vibronic peaks at 522, 555, and 600 nm, respectively, which were attributed to the intermolecular π - π interactions in the crystalline phase. P1 had similar vibronic peaks as P3HT, indicating that the addition of sulfinyl groups at the end of P3AT side chains did not significantly destroy the long-range π - π interactions. Similarly, P3 also had three vibronic peaks, though weaker than those of P3HT. On the contrary, P2 did not show obvious vibronic peaks, and possible reasons will be discussed later.

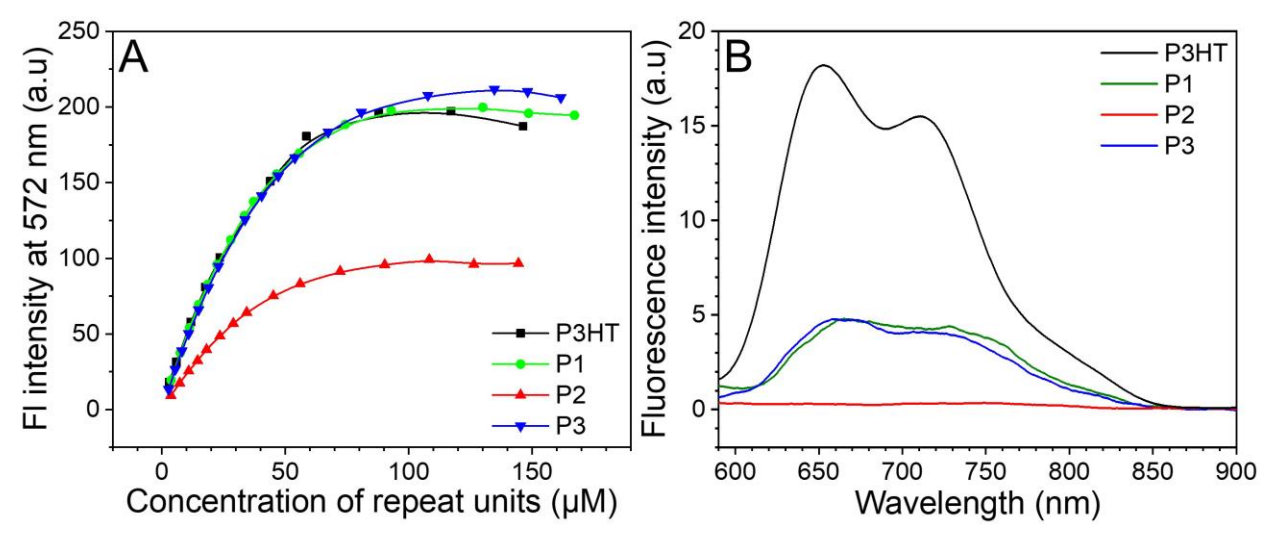


Figure 7. (A) Fluorescence intensity at 572 nm as function of the repeat-unit concentration in solution (i.e., chloroform with 6 vol.% methanol) and (B) fluorescence spectra in spin-coated thin films (~65 nm thick) for P3HT, P1, P2, and P3, respectively.

Figure 7A depicts the fluorescence intensity at 572 nm as a function of the repeat-unit concentration of functionalized P3AT polymers in solution. Although all polymers exhibited the same normalized fluorescence spectra in solution (see Figure S15), the fluorescence intensity at 572 nm appeared to be different for different polymers. From Figure 7A, fluorescence intensities of all polymers had a linear relationship with the repeat-unit concentration when the concentration was below ~20 μM. Upon further increasing the repeat-unit concentration, fluorescence intensities started to level off and reached a plateau value. The plateau fluorescence intensities of P3HT, P1, and P3 were similar, i.e., around 195 a.u. However, P2 exhibited a much lower plateau fluorescence intensity, only 95 a.u., nearly half of those for P3HT, P1, and P3. Film fluorescence of these polymers was measured to investigate how functional groups affect the emission in the solid state (Figure 7B). Even though all spin-coated films had a similar thickness (~65 nm) and were measured under the same conditions, large differences in the fluorescence intensity were observed depending on the polar groups in side chains. P3HT had the strongest fluorescence intensity, followed by P1 and P3 with similar but much lower fluorescence intensities and P2 with

negligible fluorescence emission. Obviously, the fluorescence-quenching effect was amplified for P1-P3 in films with P2 almost completely quenched. For P1 and P3, sulfinyl and sulfonyl groups in the side chains appeared to interact with polythiophene backbone, facilitate the vibrational relaxation, and thus attenuate the fluorescence emission. For P2, there must be an additional reason for the complete fluorescence-quenching.

Considering the large difference in polarity between polar sulfonyl side chains and hydrophobic polythiophene backbones, it is likely that micelles could form for P1-P3 in the chloroform with 6 vol.% methanol. Consequently, this might affect the optical properties of functionalized P3AT polymers.^{39, 40} To test this speculation, AFM was used to study the surface morphologies of solution-cast films for P3HT and P1-P3 (see Figure S16). The surfaces of P3HT and P1 were relatively smooth without any signs of micelle formation, whereas P2 and P3 films showed typical micellar morphology with average micelle sizes around 50-100 nm. Giving the fact that P1 and P3 films showed similar fluorescence intensity (Figure 7B) while P3 formed micelles and P1 did not form micelles in films, micelle formation could not explain fluorescence-quenching observed for solid film.

Wei et. al. found that oxidized thiophene units in the polythiophene main chain could drastically decrease the fluorescence in solutions.⁴¹ Since the fluorescence of P2 was significantly lower both in solution and film compared to other polymers, we surmise that P2 might contain intrinsic defects in the polymer backbone, such as oxidized thiopeneic units. Note that *m*-CPBA was used to oxidize thiophene at room temperature.⁴² Although it took a long time for the thiophene oxidization to happen, it was still possible that a small amount of thiophenic units in P-MeST was oxidized by *m*-CPBA during the reaction. Careful inspection of the ¹H NMR spectrum of P2 in Figure S8A confirmed a small amount of oxidized thiophenic units: the integral of proton

on the thiophenic unit (peak a, 0.91) was lower than the expected value of 1.0, and a small peak around 7.5 ppm was seen. To help assign this peak, an overoxidized P2 was purposely synthesized by reacting 4 equivalents of *m*-CPBA with P-MeST, and ¹H NMR of the overoxidized P2 is shown in Figure S8B. The proton signal around 7.5 ppm was larger, and is assigned to the proton on the oxidized thiophenic units. ⁴³ In addition, the proton signal (peak a') from oxidized thiophenic units and the peak for CH₂ protons adjacent to the oxidized thiophenic unit (i.e., peak b in Figure S8B) were also observed. To study the effect of the intrinsic defects in P2 on fluorescence quenching, we blended P3HT with P2 at different ratios. As shown in Figures S17A and B, the fluorescence emission gradually quenched and the vibronic peaks gradually disappeared upon addition of P2 into P3HT in thin films. In this case, it is likely that P2 and P3HT formed miscible blends in the solid state, and that the oxidized defects in P2 caused weakening of vibronic peaks and quenching of fluorescence.

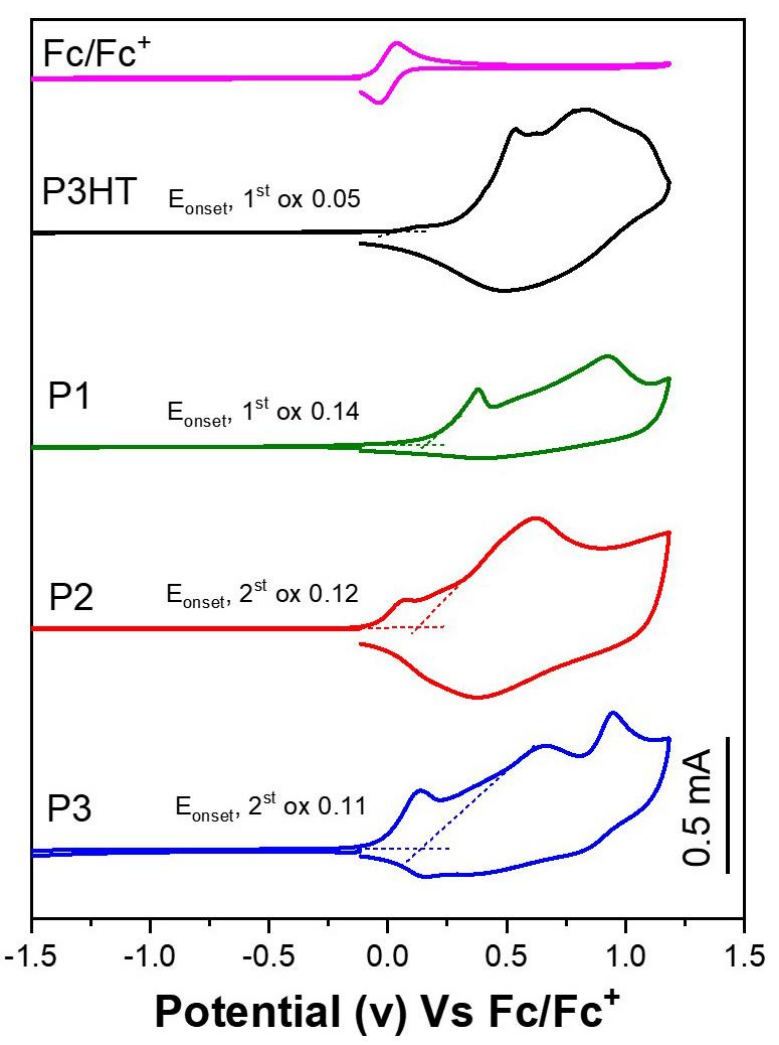


Figure 8. Thin film cyclic voltammetry (CV) curves for P3HT, P1, P2 and P3, respectively. Fc/Fc⁺ was used as internal standard.

Electrochemical Properties. Figure 8 depicts the cyclic voltammograms (CV) of P3HT and the functionalized P3AT polymers in thin films. The oxidation onset potentials were used to estimate the HOMO energy levels. For P3HT, the small peak around 0.1 V was considered as the first oxidation peak and the first onset oxidation potential versus Fc/Fc⁺ was calculated to be 0.05 V. From this onset, the HOMO energy level of P3HT was estimated to be -5.15 eV.⁴⁴ For P1, the first onset oxidation potential versus Fc/Fc⁺ was 0.14 V and the HOMO energy level was estimated to be -5.24 eV. For P2 and P3, there existed a first oxidation peak ~ 0.1 V, which was more positive than expected for oxidation of the polythiophene backbone. To elucidate the nature of

this oxidation, we measured the CV spectra of P2, P3, and R-P3, a small molecule that contained sulfonyl groups in DMF, as shown in Figure S18. Ethyl acetate (which contains an ester group) and dimethyl sulfoxide (which contains a sulfinyl group) both did not show any peaks in the measurable spectrochemical window. On the other hand, molecule R-P3 (which contains a sulfonyl group) had an oxidation peak ~0.26 V, very similar to the first oxidation peaks observed for P2 and P3 in solution. Therefore, we attribute the first oxidation peak to oxidation of the sulfonyl groups in P2 and P3. To estimate the HOMO energy levels of P2 and P3, we therefore used the second onset of the oxidation potentials versus Fc/Fc⁺, and they were 0.12 V for P2 and 0.11 V for P3. The corresponding HOMO energy levels were estimated to be -5.22 and -5.21 eV for P2 and P3, respectively. The lowest unoccupied molecular orbital (LUMO) energy levels were estimated using the optical band gap (Eg,opt) values and are reported in Table 1.

Dielectric Properties. It is difficult to accurately measure the dielectric constant of semiconducting polymers, because conduction of space charges (i.e., electrons and holes, and sometimes impurity ions) can significantly prevent the accurate measurement of the capacitance from electronic, atomic, and dipolar polarizations.^{15, 16} First, directly sandwiching the semiconductor between two metal electrodes [or with a poly(3,4-ethylenedioxythiophene)-polystyrene sulfonate (PEDOT-PSS) hole-conducting/electron-limiting layer] should not be used to measure dielectric constants by BDS or impedance spectroscopy, because the high conductance of mobile space charges shorts the sample, especially at low frequencies. To prevent the direct shorting of the sample from space charge conduction, at least a bilayer structure comprised of a semiconducting polymer and a highly insulating dielectric layer such as SiO₂ should be used, as reported in the literature.²³

In this study, we tested this method for P3HT and P1-P3. A gold/semiconducting polymer/SiO₂/n-doped Si device was used following the literature report.²³ The n-Si substrate and the gold coating served as conductive electrodes. The SiO₂ layer was made by wet-etching chemistry, rather than the dry O₂ oxidation method. It had a thickness of 230±10 nm and was used as the insulating dielectric layer to block the leakage current from space charges in the semiconducting polymer. Compared to the thin SiO₂ layer, a thick (5-10 μ m) polymer film was drop cast on the top of the SiO₂ layer. In such a way, the capacitance of the semiconducting polymer layer (C_p) was smaller than that of the SiO₂ layer (C_{Si}). Without any conduction of space charges, the measured bilayer capacitance (C) is: $1/C = 1/C_p + 1/C_{Si}$. Because C_p is smaller than C_{Si}, the bilayer C is close to C_p and the system errors from surface roughness and pinholes in the semiconducting polymer layer can be minimized.

The bottom n-Si wafer was a continuous electrode (ca. 1 in²). The top gold electrode had a discrete circular shape with a diameter of 2.4 mm. In such a configuration, there was a problem of conduction when the semiconducting polymer layer was a continuous film. Because the SiO₂ layer was prepared from wet-etching chemistry, there were some pinholes with an estimated density of 1 per 10-20 mm². With a continuous semiconducting polymer layer, the top gold electrode could short-circuit with the bottom n-Si electrode through the continuous polymer layer. To avoid this problem, the polymer was isolated by carefully wiping off the polymer around the top gold electrode using a cotton swab soaked with acetone. By doing so, we were able to obtain about 5-6 successful devices out of 10 samples for the dielectric constant measurement.

One way to eliminate the effect of space charge conduction is to apply a DC bias voltage to the bilayer capacitor in order to deplete space charges in the semiconducting polymer layer (i.e., by recombination of electrons from the negative gold electrode and holes in the *p*-type polymer),

while measuring the bilayer capacitance using a sinusoidal driving voltage (the root-mean square voltage, V_{rms} = 1 V), as described in a previous report.²³ Then, C_p and thus dielectric constant of the semiconducting polymer can be extracted from the bilayer capacitance, when space charges are depleted. To test the suitableness of this idea, the capacitance of the P3HT/SiO₂ bilayer capacitor was measured by sweeping the bias voltage from -50 to +150 V at room temperature with different frequencies of the measuring AC voltage (1 V_{rms}), as shown in Figure S19. When the bias voltage was negative, the capacitance remained constant (ca. 6.1×10⁻¹⁰ F), which was the capacitance of the SiO₂ layer $[C_{Si} = \varepsilon_{r,Si}\varepsilon_0 A/d = 6.15\times 10^{-10}]$ F, where $\varepsilon_{r,Si}$ is the relative permittivity of SiO₂ (4.0, and also see our BDS data in Figure S20, ε_0 is the vacuum permittivity, A is the sample area (4.52 mm²), and d is the thickness of the SiO₂ layer]. When the bias voltage changed to positive values (see Figure S19A), the bilayer capacitance started to drop, indicating that holes in the P3HT layer were gradually depleted by the electrons from the negative gold electrode. However, the bilayer capacitance did not reach a saturation even when the bias voltage was 100 V (see Figure S19B). Using the capacitance value at 100 V bias voltage, the dielectric constant for P3HT was calculated to be 2.9, which is lower than the literature value of 3.8.45 This measurement method was also applied to functionalized P3HT samples (i.e., P1-P3); however, complete depletion of holes could not be reached even when the bias voltage was as high as 200 V (data not This result indicated that this method could not be generalized for different shown). semiconducting polymers. In addition, a high bias voltage should be avoided for dielectric measurements because of the high risk for dielectric breakdown. For example, breakdown was observed at 10 Hz when the bias voltage increased to 50 V and above in Figure S19B.

Rather than using a high DC bias voltage, a high frequency could be used to stop the conduction of space charges, because it is known that above a certain frequency, migration of

impurity ions in a polar polymer vanishes. 46 In other words, low-voltage BDS could be directly used to measure the dielectric constant of semiconducting polymers for the bilayer sample geometry in Figure S19A. Figures S21A,B show frequency-scan BDS results for the real (C') and imaginary (C") parts of the measured complex capacitance (C*) of the bilayer P3HT/SiO₂ sample. When the pristine sample was measured in air, the C' reached a maximum value of 6.1×10⁻¹⁰ F below 10² Hz and a minimum value of 2×10⁻¹¹ F above 10⁵ Hz, respectively. Again, the low frequency C' value was the same as that of the SiO₂ layer, indicating that P3HT became conductive at low frequencies due to the high mobility of holes. Above 10⁵ Hz, holes could not catch up with the fast switching AC voltage, leading to series capacitors of SiO2 and P3HT. Between these two frequencies, holes started to migrate and P3HT gradually lost the capability of storing electric energy. From the bilayer capacitance, the dielectric constant of P3HT at room temperature was calculated to be 3.75, which is consistent with the reported value.⁴⁵ However, the window for series SiO₂ and P3HT capacitors was rather narrow, only from 10⁵ to 10⁶ Hz. To broaden this frequency window, thermal annealing at 100 °C for 1 h was carried out in a dry N2 atmosphere (i.e., in the Novocontrol sample chamber). After annealing, the frequency window extended down to 10 Hz. Meanwhile, there was a peak observed in the C" plot in Figure S21B, which could be attributed to the conduction of holes in P3HT.⁴⁷ This conduction peak shifted from 300 Hz for the sample in air to 0.3 Hz for the thermally annealed sample in N₂. Similar peaks were also observed for the conduction of impurity ions in polar polymers such as poly(vinylidene fluoride) (PVDF), and the peak position was related to the mobility of impurity ions.^{48, 49} Therefore, the shift of the C" peak to a lower frequency after thermal annealing in N₂ might suggest that the hole mobility decreased after removing O₂ from the sample. Namely, P3HT was de-doped. While O₂ doping of P3HT is known to increase conductivity via introducing more holes into the polymer, ⁵⁰ it has also

been shown to improve mobility.⁵¹ A similar doping effect on charge carrier mobility was also reported for high dielectric constant 2D molybdenum oxide.⁵² For the rest of this dielectric study, all samples (P3HT and P1-P3) were thermally annealed at 100 °C for 1 h in order to minimize O₂-doping. By lowering the temperature, the hole mobility further decreased and the hole conduction peak continuously shifted to lower frequencies, as shown in Figures S19C,D. Nonetheless, the dielectric constant of P3HT changed only slightly between 3.6 and 4.0.

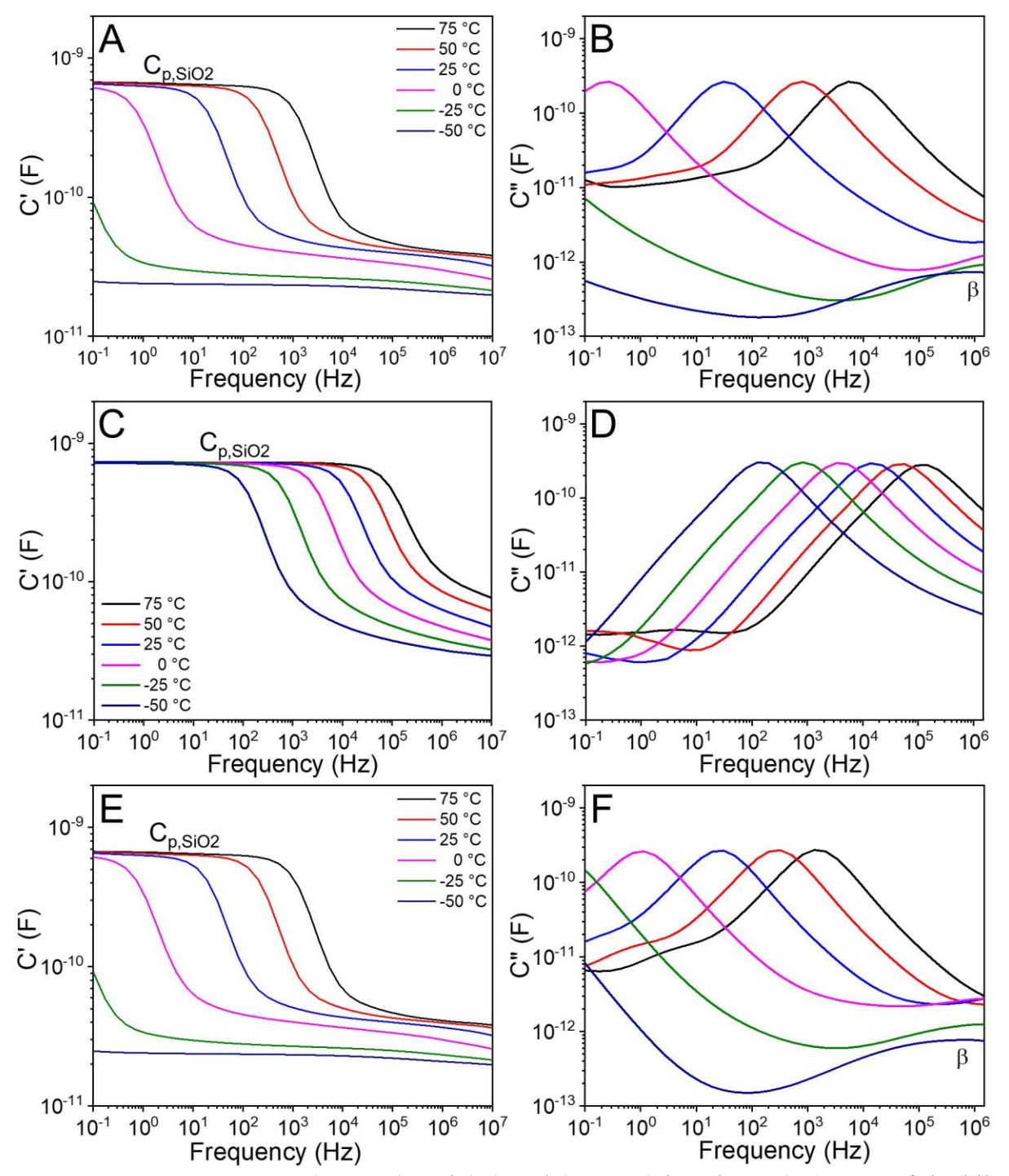


Figure 9. Frequency-scan (A, C, E) real (C') and (B, D, F) imaginary (C") parts of the bilayer capacitance at various temperatures for (A, B) P1, (C, D) P2, and (E, F) P3, respectively. The layer thicknesses for P1, P2, and P3 are 9.3, 9.3, and 8.1 μm, respectively. The standard deviation of film thicknesses was around 10%.

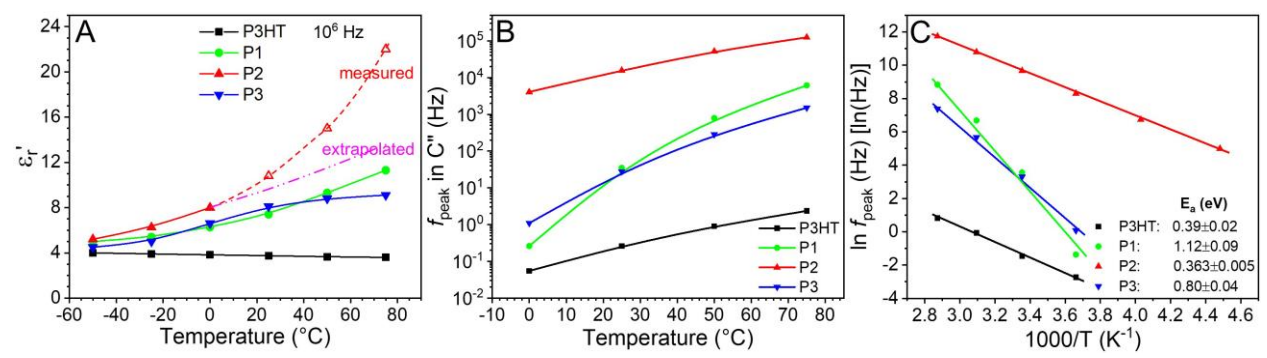


Figure 10. (A) Dielectric constants as a function of temperature for P3HT, P1, P2, and P3, calculated from the C' values at 10^6 Hz in Figures S19C and 9A,C,E. (B) Ln f as a function of 1/T for P3HT, P1, P2, and P3. The activation energy (E_a) values are calculated from the slopes in (C).

Frequency-scan BDS was applied to P1, P2, and P3 at different temperatures, and results are shown in Figure 9. Similar to the case for P3HT in Figure S21, dielectric constants of P1-P3 could be calculated from the C' values at 10⁶ Hz, as long as the C' had almost reached the plateau value (i.e., free of the influence from hole migration/conduction). Figure 10A summarizes calculated dielectric constants at different temperatures for P3HT and P1-P3. At -50 °C (and below), the dielectric constants of all sample were similar, i.e., around 4-5, indicating that dipolar polarization in P1-P3 should be largely suppressed (i.e., dipoles were mostly frozen). Upon increasing the temperature, the dielectric constant for P3HT slightly decreased to 3.6 at 75 °C. On the contrary, dielectric constants for P1-P3 increased with temperature. The dielectric constants for P1 and P3 were similar, whereas that for P2 was higher. Note that at 25 °C and above, the C' for P2 did not reach the minimum plateau values due to a higher conduction or possibly a higher hole mobility. Therefore, the calculated dielectric constant for P2 at 25 °C and above were not accurate, and the data are represented by the open triangle symbol in Figure 10A. To obtain a more accurate dielectric constant, an extrapolated curve was used (see the magenta curve in Figure 10A). At room temperature, the dielectric constants for P1, P2, and P3 were 7.4, 8.1, and 9.3, respectively, significantly higher than that of P3HT. The higher dielectric constant for P2 than P1

could be attributed to the larger dipole moment for the sulfonyl group (4.5 D) than that of the sulfinyl group (3.95 D). The lower dielectric constant for P3 than P2 could be attributed to the twisted conformation of side chains, where the dipole moments from ester and sulfonyl groups might cancel each other.

From Figure 10, the dielectric behaviors of P1 and P3 appeared to be similar, whereas P2 behaved differently. Basically, at the same temperature, the hole-conduction peak frequencies in C" for P1 and P3 were similar, whereas the peak in C" for P2 appeared at much higher frequencies (data is also summarized in Figure 10B). Nonetheless, all conduction peak frequencies for P1-P3 were higher than that for P3HT (see Figure S21). Because the conduction peak position in C" was not very sensitive to the polymer thickness as long as they were similar, we surmise that it should be primarily related to the hole mobility in samples. Consequently, the results in Figure 10B suggest that the hole mobilities in P1-P3 were higher than that of P3HT. Also, the hole mobilities of P1 and P3 were similar, but lower than that of P2. This observation correlated well with the order of dielectric constants for P3HT and P1-P3, as observed in Figure 10A. We consider that there should a correlation of dielectric constant with charge carrier mobility; the higher the dielectric constant, the higher the charge carrier mobility. This is consistent with the idea or proposal in our previous publication.¹⁹ Increased charge carrier mobility with higher dielectric constant has also been observed for 2D molybdenum oxide.⁵² To better quantify the charge carrier mobilities, we are currently working on theoretical simulation of the bilayer system, and results will be published in the future. Note that in Figures 8B and F, the sub- $T_{\rm g}$ or β transition from dipole switching were observed around 10⁶ Hz for P1 and P3, respectively. However, the β transition was not observed for P2 because the fast hole conduction masked it.

The temperature dependence of charge carrier mobility was studied by the $\ln f_{\rm peak}$ vs. 1/T plot in Figure 10C. Linear Arrhenius relationship was observed, and from the slopes the activation energy (E_a) was obtained. The E_a values for P1 and P3 were around 0.8-1.12 eV whereas those for P3HT and P2 were around 0.36-0.39 eV. These values were similar to the E_a for conduction of impurity ions in PVDF.⁴⁶ The higher E_a values for P1 and P3 indicated that the mobilities for P1 and P3 were more temperature dependent than those for P3HT and P2.

Conclusions

In this work, we have successfully synthesized functionalized P3AT polymers with highly dipolar methylsulfinyl or methylsulfonyl end groups in the alkyl side chains. The goal is to achieve high ε_r via enhanced dipolar polarization without significantly changing the crystalline structure for the polythiophene backbones. Structural analysis based on GI-WAXD indicated that the crystalline structure of polythiophene backbones was largely preserved, although the overall crystallinity was somewhat interfered by the strong dipolar interaction among the sulfinyl and sulfonyl end groups. Using a bilayer sample geometry, the ε_r of these semiconducting polymers were accurately determined by frequency-scan BDS at various temperatures. Indeed, the ε_r values of P1, P2, and P3 increased from 3.75 for P3HT to 7.4, 9.3, and 8.1, respectively, at 1 MHz and room temperature. To the best of our knowledge, these are amongst the highest ε_r values based on reliable measurements reported for conjugated polymers. At this moment, we speculate that both sulfinyl/sulfonyl groups in the amorphous phase and in the crystals should contribute to the high dielectric constant of P1-P3.

Although the P3HT crystalline structure and the conjugation length was largely preserved for the side chain-functionalized P1-P3, the highly interacting sulfinyl and sulfonyl groups should

have facilitated the vibrational relaxation of the polythiophene backbones, resulting in the

weakened vibronic absorption bands in UV-Vis and decreased fluorescence intensity for thin films.

In particular, P2 largely lost the vibronic bands and fluorescence was quenched in the solid state.

This was attributed to the slight oxidation of the polythiophene units in the main chain of P2. In

this sense, P1 with sulfinyl groups had a lower impact on optical properties in thin films than P2

with sulfonyl groups, suggesting that methylsulfinyl end groups may provide a balance between

obtaining high ε_r and preserving favorable π - π interaction for the polythiophene backbones.

Research is currently underway to explore the charge transport properties (i.e., charge

concentration and mobility) of P1-P3 using combined broadband dielectric spectroscopy and

computer simulation, and device performance will be reported in the future.

Author Information

Corresponding Authors

*E-mail: lxz121@case.edu (L.Z.)

*E-mail: gxs244@case.edu (G.S.)

ORICD

Chunlai Wang: 0000-0002-3519-4293

Zhongbo Zhang: 0000-0001-5294-444X

Lei Zhu: 0000-0001-6570-9123

Genevieve Sauve: 0000-0002-9721-0447

Notes

36

The authors declare no competing financial interest.

Acknowledgements

We are grateful to the National Science Foundation (NSF, CHEM-1148652) for funding this project. BDS characterization by ZZ and LZ is supported by NSF, Division of Materials Research (DMR), Polymers Program (DMR-1708990). We thank Dr. Forrest Etheridge for advice on synthesis; Dr. Eric Baer for DSC measurement; Dr. James Burgess for facilitating cyclic voltammetry, and Dr. Emily Pentzer for providing access to UV-Vis instrument. MALDI-TOF instrument was supported by NSF under Grant MRI-0821515. GI-WAXD experiments were performed at the 11-BM CMS beamline of NSLS-II, BNL, a U.S. Department of Energy User Facility operated for the Office of Science by BNL under Contract DESC0012704.

¹H NMR spectra of small molecules and polymers; MALDI-TOF of polymers; AFM images of P3HT, P1, P2, and P3 solution-cast thin films; fluorescence and UV-Vis spectra of blends in films; cyclic voltammetry of P2 and R-P3 in DMF; dielectric characterization of P3HT/SiO₂ bilayer.

References

Miyata, A.; Mitioglu, A.; Plochocka, P.; Portugall, O.; Wang, J. T. W.; Stranks, S. D.; Snaith,
 H. J.; Nicholas, R. J. Direct Measurement of the Exciton Binding Energy and Effective

- Masses for Charge Carriers in Organic-Inorganic Tri-Halide Perovskites. *Nat. Phys.* **2015**, *11*, 582-587.
- 2. Kraner, S.; Scholz, R.; Koerner, C.; Leo, K. Design Proposals for Organic Materials Exhibiting a Low Exciton Binding Energy. *J. Phys. Chem. C* **2015**, *119*, 22820-22825.
- 3. Green, M. A.; Ho-Baillie, A.; Snaith, H. J. The Emergence of Perovskite Solar Cells. *Nat. Photonics* **2014**, *8*, 506-514.
- 4. Poglitsch, A.; Weber, D. Dynamic Disorder in Methylammoniumtrihalogenoplumbates (II) Observed by Millimeter-Wave Spectroscopy. *J. Chem. Phys.* **1987**, *87*, 6373-6378.
- Miyata, K.; Meggiolaro, D.; Trinh, M. T.; Joshi, P. P.; Mosconi, E.; Jones, S. C.; De Angelis,
 F.; Zhu, X. Y. Large Polarons in Lead Halide Perovskites. *Sci. Adv.* 2017, 3, e1701217.
- 6. Frost, J. M.; Butler, K. T.; Brivio, F.; Hendon, C. H.; van Schilfgaarde, M.; Walsh, A. Atomistic Origins of High-Performance in Hybrid Halide Perovskite Solar Cells. *Nano Lett.* **2014**, *14*, 2584-2590.
- 7. Nayak, P. K. Exciton Binding Energy in Small Organic Conjugated Molecule. *Synth. Met.* **2013**, *174*, 42-45.
- 8. Dkhissi, A. Excitons in Organic Semiconductors. Synth. Met. 2011, 161, 1441-1443.
- 9. Hummer, K.; Ambrosch-Draxl, C. Oligoacene Exciton Binding Energies: Their Dependence on Molecular Size. *Phys. Rev. B* **2005**, *71*, 081202.
- van der Horst, J. W.; Bobbert, P. A.; Michels, M. A. J.; Bassler, H. Calculation of Excitonic Properties of Conjugated Polymers Using the Bethe-Salpeter Equation. *J. Chem. Phys.* 2001, 114, 6950-6957.

- 11. Zhang, G.; Clarke, T. M.; Mozer, A. J. Bimolecular Recombination in a Low Bandgap Polymer:PCBM Blend Solar Cell with a High Dielectric Constant. *J. Phys. Chem. C* **2016**, *120*, 7033-7043.
- 12. Koster, L. J. A.; Shaheen, S. E.; Hummelen, J. C. Pathways to a New Efficiency Regime for Organic Solar Cells. *Adv. Energy Mater.* **2012,** *2*, 1246-1253.
- Torabi, S.; Jahani, F.; Van Severen, I.; Kanimozhi, C.; Patil, S.; Havenith, R. W. A.; Chiechi,
 R. C.; Lutsen, L.; Vanderzande, D. J. M.; Cleij, T. J.; Hummelen, J. C.; Koster, L. J. A.
 Strategy for Enhancing the Dielectric Constant of Organic Semiconductors Without
 Sacrificing Charge Carrier Mobility and Solubility. Adv. Funct. Mater. 2015, 25, 150-157.
- 14. Brebels, J.; Manca, J. V.; Lutsen, L.; Vanderzande, D.; Maes, W. High Dielectric Constant Conjugated Materials for Organic Photovoltaics. *J. Mater. Chem. A* **2017**, *5*, 24037-24050.
- 15. Zhu, L. Exploring Strategies for High Dielectric Constant and Low Loss Polymer Dielectrics. *J. Phys. Chem. Lett.* **2014**, *5*, 3677-3687.
- 16. Kremer, F.; Schönhals, A. Broadband Dielectric Spectroscopy; Springer: Berlin, 2003.
- 17. Baer, E.; Zhu, L. 50th Anniversary Perspective: Dielectric Phenomena in Polymers and Multilayered Dielectric Films. *Macromolecules* **2017**, *50*, 2239-2256.
- 18. Wang, C. C.; Pilania, G.; Boggs, S. A.; Kumar, S.; Breneman, C.; Ramprasad, R. Computational Strategies for Polymer Dielectrics Design. *Polymer* **2014**, *55*, 979-988.
- 19. Zhao, Z.; Zhang, Z.; Pejic, S.; Zhang, G.; Zhu, Y.; Liu, H.; Litt, M.; Sauve, G.; Zhu, L. Synergistic Dielectric and Semiconducting Properties in Fluorescein Monopotassium Salt Random Copolymers. *Polymer* **2017**, *114*, 189-198.

- de Gier, H. D.; Broer, R.; Havenith, R. W. A. Non-Innocent Side-Chains with Dipole Moments in Organic Solar Cells Improve Charge Separation. *Phys. Chem. Chem. Phys.* 2014, 16, 12454-12461.
- 21. Yang, P.; Yuan, M.; Zeigler, D. F.; Watkins, S. E.; Lee, J. A.; Luscombe, C. K. Influence of Fluorine Substituents on the Film Dielectric Constant and Open-Circuit Voltage in Organic Photovoltaics. *J. Mater. Chem. C* **2014**, *2*, 3278-3284.
- Cho, N.; Schlenker, C. W.; Knesting, K. M.; Koelsch, P.; Yip, H. L.; Ginger, D. S.; Jen, A.
 K. Y. High-Dielectric Constant Side-Chain Polymers Show Reduced Non-Geminate Recombination in Heterojunction Solar Cells. Adv. Energy Mater. 2014, 4, 1301857.
- Armin, A.; Stoltzfus, D. M.; Donaghey, J. E.; Clulow, A. J.; Nagiri, R. C. R.; Burn, P. L.;
 Gentle, I. R.; Meredith, P. Engineering Dielectric Constants in Organic Semiconductors. *J. Mater. Chem. C* 2017, 5, 3736-3747.
- 24. Kao, K.-C. Dielectric Phenomena in Solids: with Emphasis on Physical Concepts of Electronic Processes; Elsevier Academic Press: Boston, 2004.
- 25. Wei, J.; Zhang, Z.; Tseng, J.-K.; Treufeld, I.; Liu, X.; Litt, M. H.; Zhu, L. Achieving High Dielectric Constant and Low Loss Property in a Dipolar Glass Polymer Containing Strongly Dipolar and Small-Sized Sulfone Groups. ACS Appl. Mater. Interfaces 2015, 7, 5248-5257.
- Zhang, Z.; Wang, D. H.; Litt, M. H.; Tan, L.-S.; Zhu, L. High-Temperature and High-Energy-Density Dipolar Glass Polymers Based on Sulfonylated Poly(2,6-dimethyl-1,4phenylene oxide). *Angew. Chem. Int. Ed.* 2018, 57, 1528-1531.
- Zhu, Y.-F.; Zhang, Z.; Litt, M. H.; Zhu, L. High Dielectric Constant Sulfonyl-Containing Dipolar Glass Polymers with Enhanced Orientational Polarization. *Macromolecules* 2018, 51, DOI: 10.1021/acs.macromol.8b00923.

- 28. Zhai, L.; Pilston, R. L.; Zaiger, K. L.; Stokes, K. K.; McCullough, R. D. A Simple Method to Generate Side-Chain Derivatives of Regioregular Polythiophene via the GRIM Metathesis and Post-Polymerization Functionalization. *Macromolecules* **2003**, *36*, 61-64.
- 29. Armarego, W. L. F.; Chai, C. L. L. *Purification of Laboratory Chemicals*. 7th Ed.; Elsevier/Butterworth-Heinemann: Amsterdam, 2013.
- 30. Iovu, M. C.; Sheina, E. E.; Gil, R. R.; McCullough, R. D. Experimental Evidence for the Quasi-"Living" Nature of the Grignard Metathesis Method for the Synthesis of Regioregular Poly(3-alkylthiophenes). *Macromolecules* **2005**, *38*, 8649-8656.
- 31. Loewe, R. S.; Khersonsky, S. M.; McCullough, R. D. A Simple Method to Prepare Head-to-Tail Coupled, Regioregular Poly(3-alkylthiophenes) Using Grignard Metathesis. *Adv. Mater.* **1999**, *11*, 250-253.
- 32. Lanzi, M.; Paganin, L. New Regioregular Polythiophenes Functionalized with Sulfur-Containing Substituents for Bulk Heterojunction Solar Cells. *React. Funct. Polym.* **2010,** *70*, 346-360.
- Rodrigues, A.; Castro, M. C. R.; Farinha, A. S. F.; Oliveira, M.; Tome, J. P. C.; Machado,
 A. V.; Raposo, M. M. M.; Hilliou, L.; Bernardo, G. Thermal Stability of P3HT and
 P3HT:PCBM Blends in the Molten State. *Polym. Test.* 2013, 32, 1192-1201.
- Snyder, C. R.; Nieuwendaal, R. C.; DeLongchamp, D. M.; Luscombe, C. K.; Sista, P.; Boyd,
 D. Quantifying Crystallinity in High Molar Mass Poly(3-hexylthiophene).

 Macromolecules 2014, 47, 3942-3950.
- 35. Shao, M.; Keum, J.; Chen, J.; He, Y.; Chen, W.; Browning, J. F.; Jakowski, J.; Sumpter, B. G.; Ivanov, I. N.; Ma, Y.; Rouleau, C. M.; Smith, S. C.; Geohegan, D. B.; Hong, K.; Xiao,

- K. The Isotopic Effects of Deuteration on Optoelectronic Properties of Conducting Polymers. *Nat. Commun.* **2014,** *5*, 3180.
- 36. Alemseghed, M. G.; Gowrisanker, S.; Servello, J.; Stefan, M. C. Synthesis of Di-Block Copolymers Containing Regioregular Poly(3-hexylthiophene) and Poly(tetrahydrofuran) by a Combination of Grignard Metathesis and Cationic Polymerizations. *Macromol. Chem. Phys.* **2009**, *210*, 2007-2014.
- 37. Alemseghed, M. G.; Servello, J.; Hundt, N.; Sista, P.; Biewer, M. C.; Stefan, M. C. Amphiphilic Block Copolymers Containing Regioregular Poly(3-hexylthiophene) and Poly(2-ethyl-2-oxazoline). *Macromol. Chem. Phys.* **2010**, *211*, 1291-1297.
- 38. Li, W.; He, Y.-G.; Shi, S.-Y.; Liu, N.; Zhu, Y.-Y.; Ding, Y.-S.; Yin, J.; Wu, Z.-Q. Fabrication of a Multi-Charge Generable Poly(phenyl isocyanide)-*Block*-Poly(3-hexylthiophene) Rod-Rod Conjugated Copolymer. *Polym. Chem.* **2015**, *6*, 2348-2355.
- 39. Liu, N.; Qi, C.-G.; Wang, Y.; Liu, D.-F.; Yin, J.; Zhu, Y.-Y.; Wu, Z.-Q. Solvent-Induced White-Light Emission of Amphiphilic Rod-Rod Poly(3-triethylene glycol thiophene)-*Block*-Poly(phenyl isocyanide) Copolymer. *Macromolecules* **2013**, *46*, 7753-7758.
- 40. Barbarella, G.; Pudova, O.; Arbizzani, C.; Mastragostino, M.; Bongini, A. Oligothiophene-S,S-Dioxides: a New Class of Thiophene-Based Materials. *J. Org. Chem.* **1998**, *63*, 1742-1745.
- 41. Tsai, C.-H.; Chirdon, D. N.; Maurer, A. B.; Bernhard, S.; Noonan, K. J. T. Synthesis of Thiophene 1,1-Dioxides and Tuning Their Optoelectronic Properties. *Org. Lett.* **2013**, *15*, 5230-5233.
- 42. Mao, Z.; Vakhshouri, K.; Jaye, C.; Fischer, D. A.; Fernando, R.; DeLongchamp, D. M.; Gomez, E. D.; Sauve, G. Synthesis of Perfluoroalkyl End-Functionalized Poly(3-

- hexylthiophene) and the Effect of Fuorinated End Froups on Solar Cell Performance. *Macromolecules* **2013**, *46*, 103-112.
- 43. Cui, J.; Martinez-Tong, D. E.; Sanz, A.; Ezquerra, T. A.; Rebollar, E.; Nogales, A. Relaxation and Conductivity in P3HT/PC71BM Blends as Revealed by Dielectric Spectroscopy. *Macromolecules* **2016**, *49*, 2709-2717.
- Huang, H.; Chen, X.; Yin, K.; Treufeld, I.; Schuele, D. E.; Ponting, M.; Langhe, D.; Baer,
 E.; Zhu, L. Reduction of Ionic Conduction Loss in Multilayer Dielectric Films by
 Immobilizing Impurity Ions in High Glass Transition Temperature Polymer Layers. ACS
 Appl. Energy Mater. 2018, 1, 775-782.
- 45. Li, J. V.; Nardes, A. M.; Liang, Z.; Shaheen, S. E.; Gregg, B. A.; Levi, D. H. Simultaneous Measurement of Carrier Density and Mobility of Organic Semiconductors Using Capacitance Techniques. *Org Electron* **2011**, *12*, 1879-1885.
- Mackey, M.; Schuele, D. E.; Zhu, L.; Baer, E. Layer Confinement Effect on Charge Migration in Polycarbonate/Poly(vinylidene fluorid-co-hexafluoropropylene) Multilayered Films. J. Appl. Phys. 2012, 111, 113702.
- 47. Yang, L.; Allahyarov, E.; Guan, F.; Zhu, L. Crystal Orientation and Temperature Effects on Double Hysteresis Loop Behavior in a Poly(vinylidene fluoride-co-trifluoroethylene)-Graft-Polystyrene Graft Copolymer. *Macromolecules* **2013**, *46*, 9698-9711.
- 48. Lu, G.; Blakesley, J.; Himmelberger, S.; Pingel, P.; Frisch, J.; Lieberwirth, I.; Salzmann, I.; Oehzelt, M.; Di Pietro, R.; Salleo, A.; Koch, N.; Neher, D., Moderate Doping Leads to High Performance of Semiconductor/Insulator Polymer Blend Transistors. *Nat. Commun.* **2013**, *4*, 1588.

- 49. Mozer, A. J.; Sariciftci, N. S.; Pivrikas, A.; Osterbacka, R.; Juska, G.; Brassat, L.; Bassler,
 H. Charge carrier mobility in regioregular poly(3-hexylthiophene) probed by transient
 conductivity techniques: A comparative study. *Phys. Rev. B* 2005, 71, 035214.
- 50. Balendhran, S.; Deng, J.; Ou, J. Z.; Walia, S.; Scott, J.; Tang, J.; Wang, K. L.; Field, M. R.; Russo, S.; Zhuiykov, S.; Strano, M. S.; Medhekar, N.; Sriram, S.; Bhaskaran, M.; Kalantar-Zadeh, K. Enhanced Charge Carrier Mobility in Two-Dimensional High Dielectric Molybdenum Oxide. *Adv. Mater.* **2013**, *25*, 109-114.

TOC Graphics

High Dielectric Constant Semiconducting Poly(3-alkylthiophene)s from Side Chain Modification with Polar Sulfinyl and Sulfonyl Groups

Chunlai Wang, Zhongbo Zhang, Sandra Pejić, Ruipeng Li, Masafumi Fukuto, Lei Zhu,*, and Geneviève Sauvé*

P3HT,
$$\epsilon_r$$
: 3.75

P3HT, ϵ_r : 3.75

P1, ϵ_r =7.4

P2, ϵ_r =9.3

P3, ϵ_r =8.1 (RT and 1 MHz)

Supporting Information

High Dielectric Constant Semiconducting Poly(3-alkylthiophene)s from Side-Chain Modification with Polar Sulfinyl and Sulfonyl Groups

Chunlai Wang,[†] Zhongbo Zhang,^{†,‡} Sandra Pejić,[†] Ruipeng Li,[§] Masafumi Fukuto,[§] Lei Zhu,^{†,‡,*}, and Geneviève Sauvé ^{†,*}

[†] Department of Chemistry, Case Western Reserve University, Cleveland, Ohio 44106-7078, United States [‡] Department of Macromolecular Science and Engineering, Case Western Reserve University, Cleveland, Ohio 44106-7202, United States

[§] National Synchrotron Light Source II, Brookhaven National Laboratory, Upon, New York 11973, United States

^{*} Corresponding authors, E-mails: lxz121@case.edu (L.Z.) and gxs244@case.edu (G.S.).

1. ¹H NMR Spectra of Small Molecules and Polymers

Ethyl 4-(methylthio)butanoate

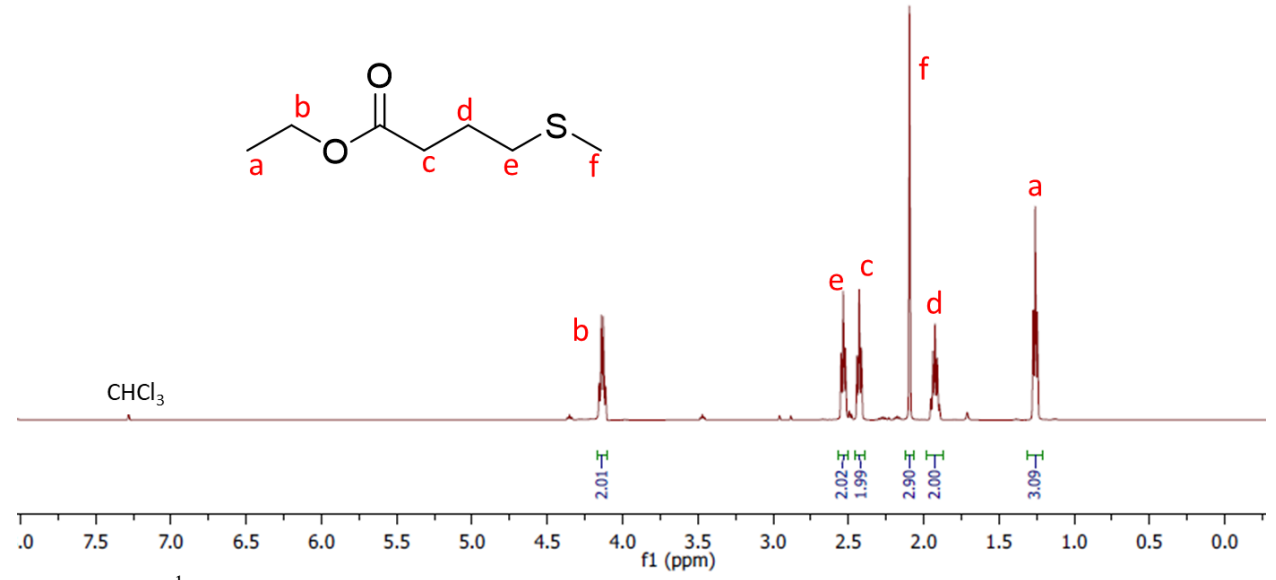


Figure S1. ¹H NMR spectrum of ethyl 4-(methylthio)butanoate. CDCl₃ was used as solvent.

4-(Methylthio)butanoic acid

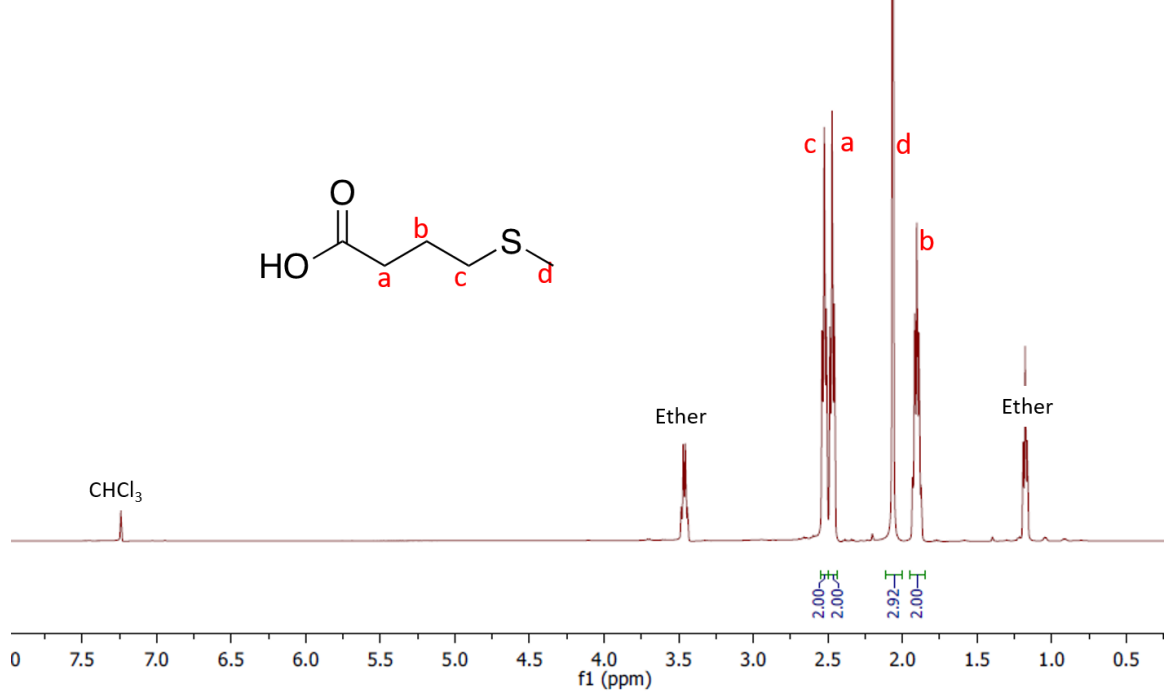


Figure S2. ¹H NMR spectrum of 4-(methylthio)butanoic acid. CDCl₃ was used as solvent. Residual diethyl ether peaks are labeled.

Sodium 4-(methylsulfonyl)butanoate (1)

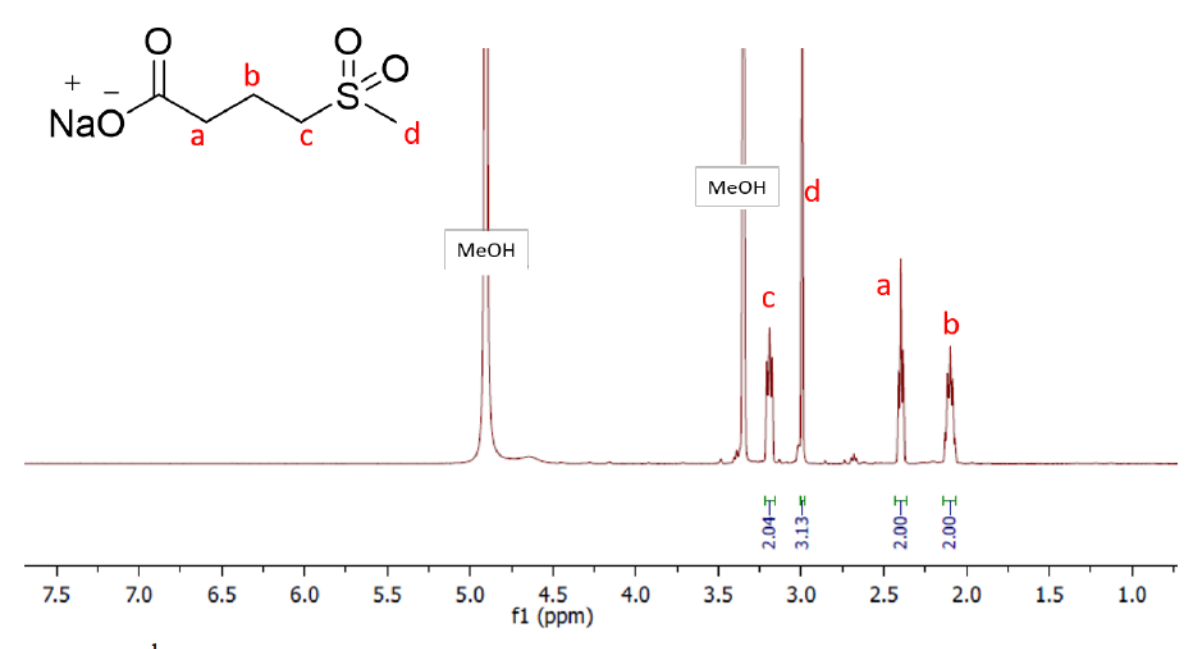


Figure S3. ¹H NMR spectrum of sodium 4-(methylsulfonyl)butanoate. MeOD was used as solvent.

Regioregular Poly(3-hexylthiophen) (P3HT)

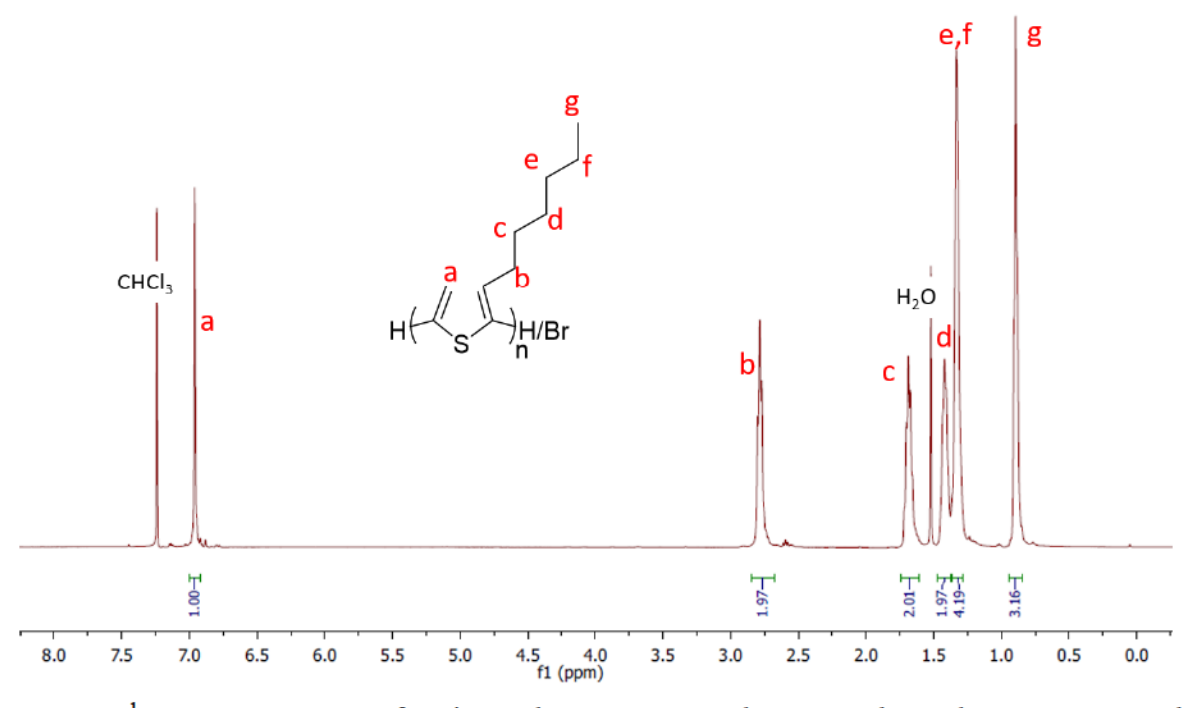


Figure S4. ¹H NMR spectrum of regionegular P3HT. CDCl₃ was used as solvent. Water peak is seen at 1.55 ppm.

Regioregular Poly[3-(6-bromohexyl) thiophene] (P-BrHT)

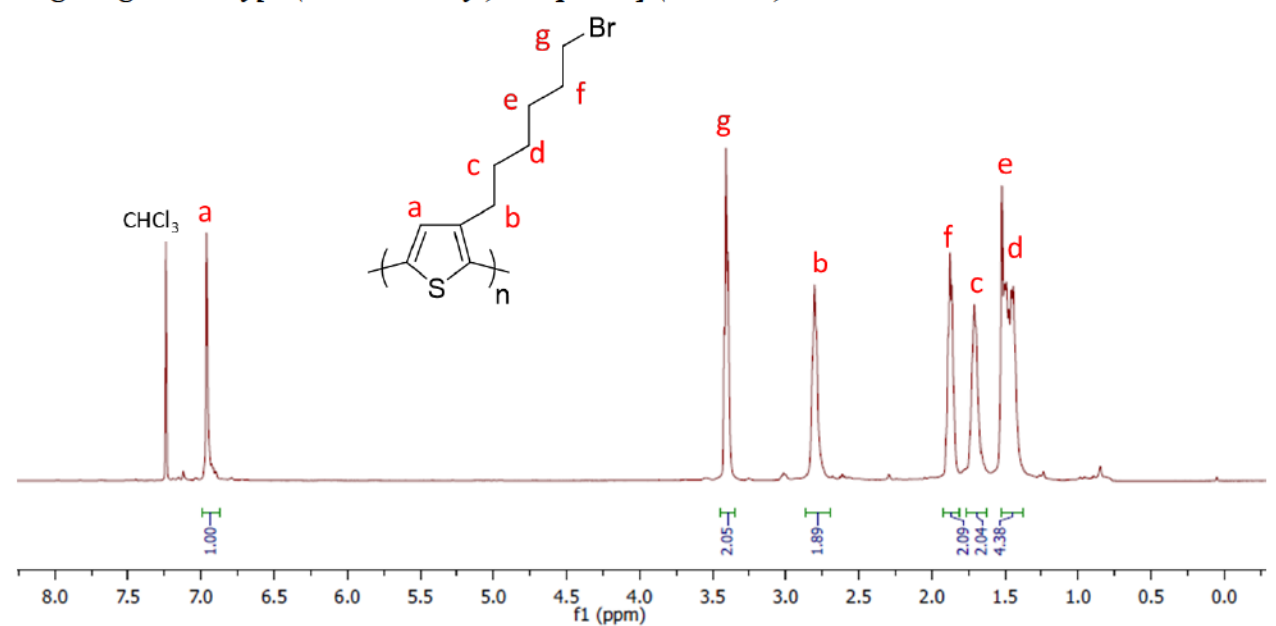


Figure S5. ¹H NMR spectrum of P-BrHT. CDCl₃ was used as the solvent. Water peak is seen at 1.55 ppm.

Poly[3-(6-methylthiolhexyl)thiophene] (P-MeST)

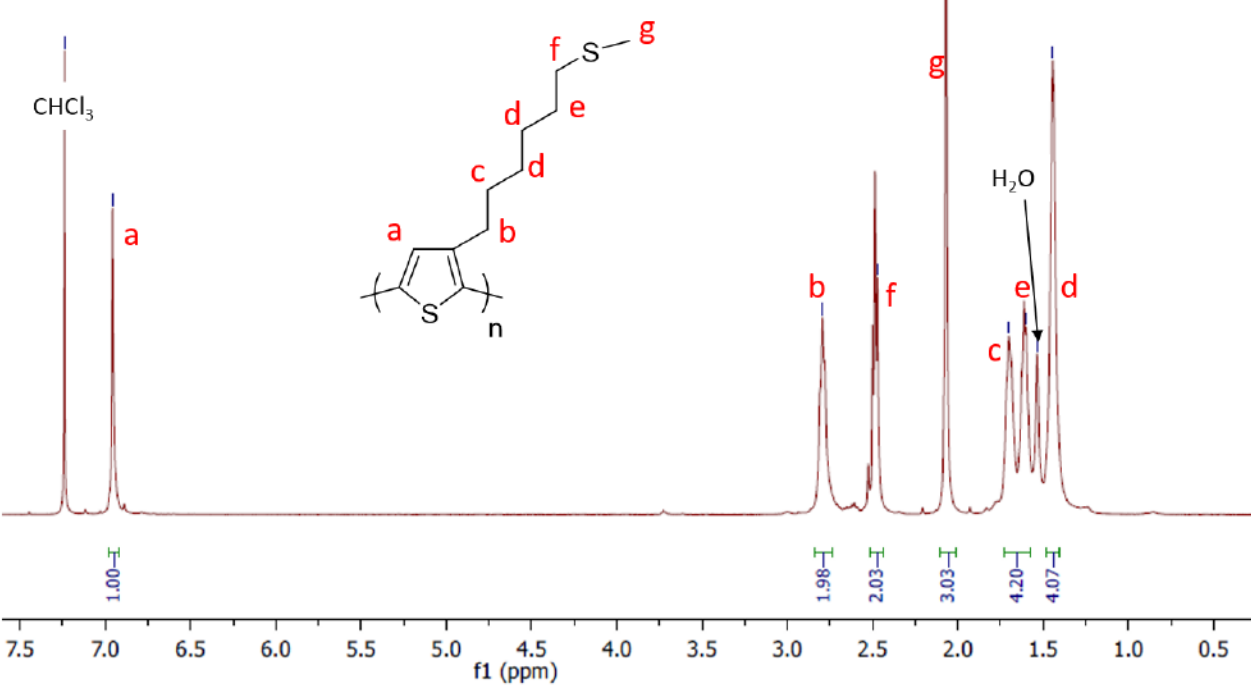


Figure S6. ¹H NMR spectrum of P-MeST. CDCl₃ was used as the solvent. Water peak is seen at 1.55 ppm.

Poly[3-(6-methylsulfinylhexyl)thiophene] (P1)

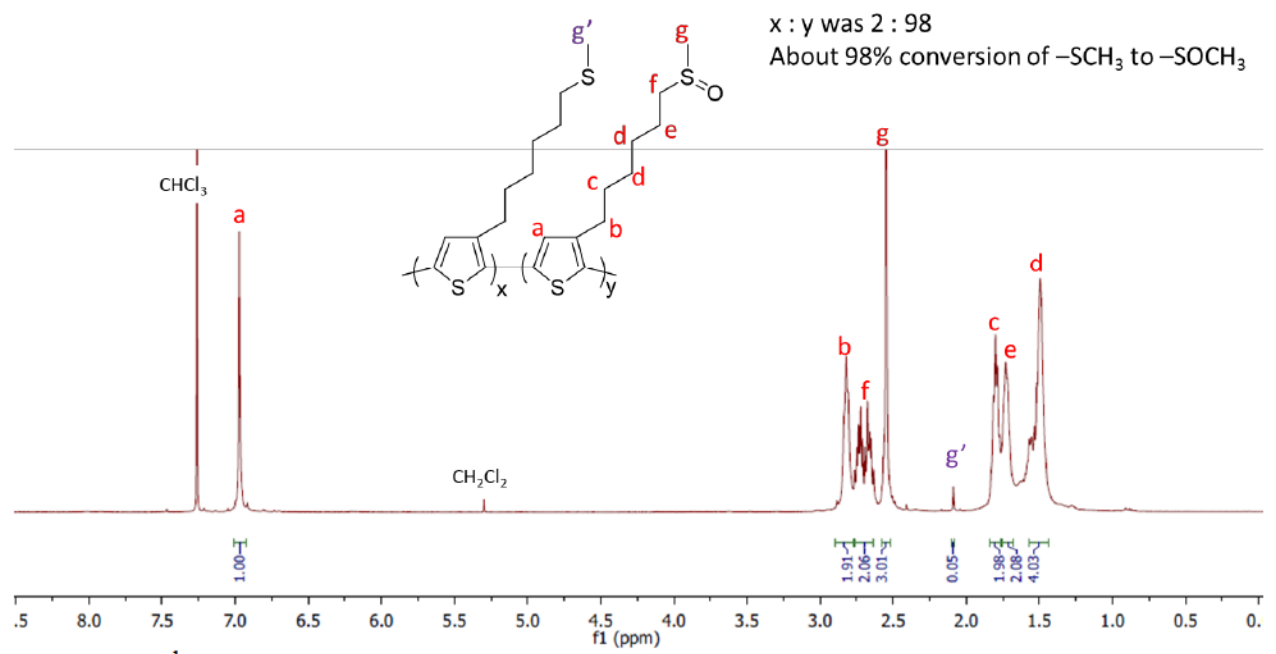
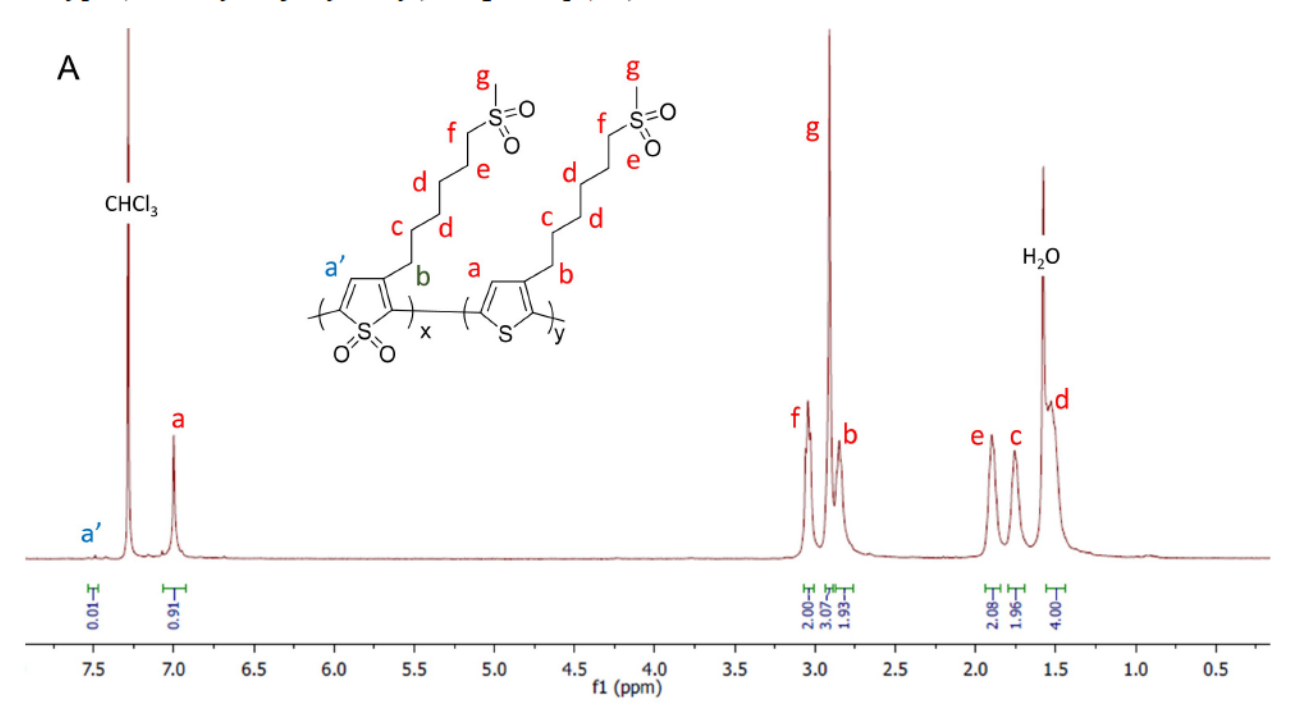


Figure S7. ¹H NMR spectrum of P1. CDCl₃ was used as the solvent.

Poly[3-(6-methylsulfonylhexyl)thiophene] (P2)



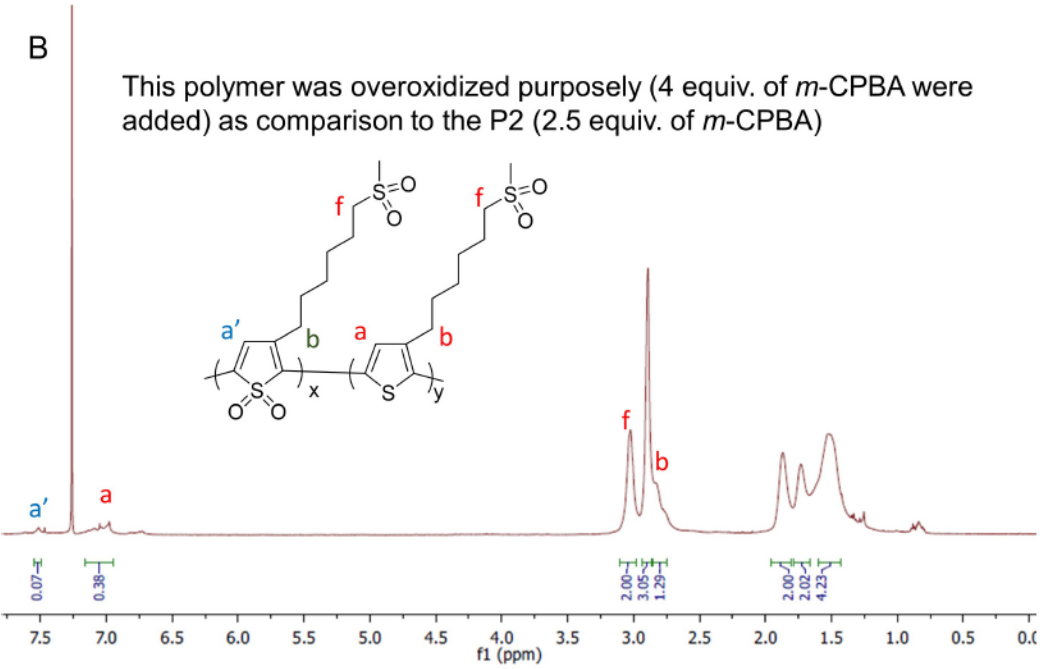


Figure S8. (A) ¹H NMR spectrum of P2. CDCl₃ was used as the solvent. Water peak is seen at 1.55 ppm. The integral for protons at f was 2.0 and integrals for other protons were normalized to it. The integral for proton a was only 0.91, smaller than the expected value of 1.0. A small peak around 7.5 ppm (peak a') is assigned to the proton on the oxidized thiophenic units. (B) ¹H NMR spectrum of overoxidized P2. CDCl₃ was used as the solvent. Proton on the oxidized thiophenic units is assigned to peak a'. Protons on the side chains that close to the oxidized thiophenic units were also affected (peak b).

Poly{3-[6-(3-methylsulfonylpropylcarbonyloxy)hexyl]thiophene} (P3)

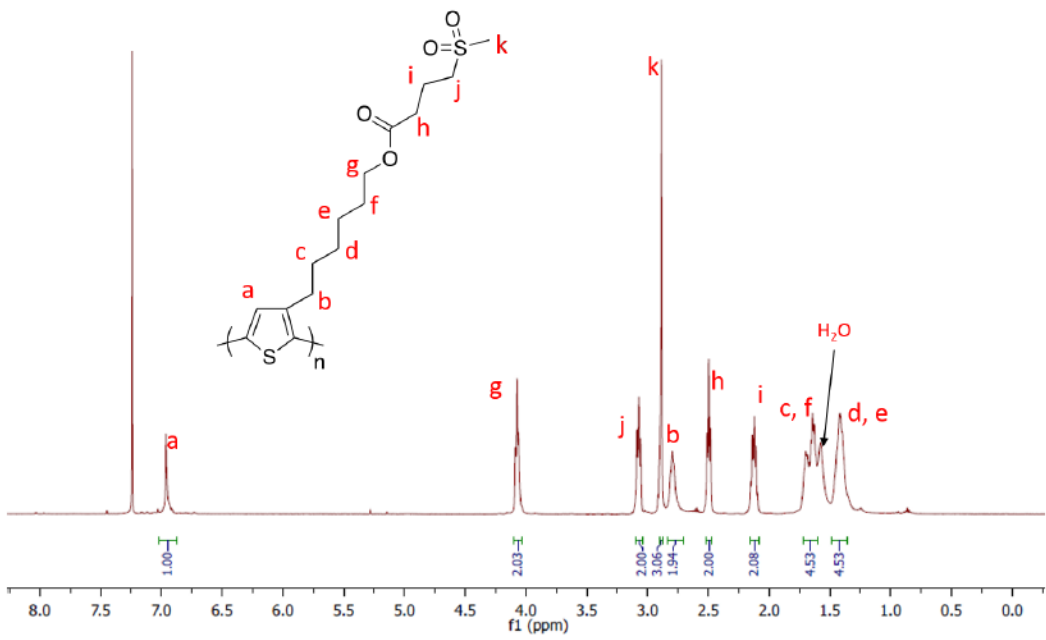


Figure S9. ¹H NMR spectrum of P3. CDCl₃ was used as the solvent. Water peak is seen at 1.55 ppm.

2. MALDI-TOF Mass Spectra of Polymers

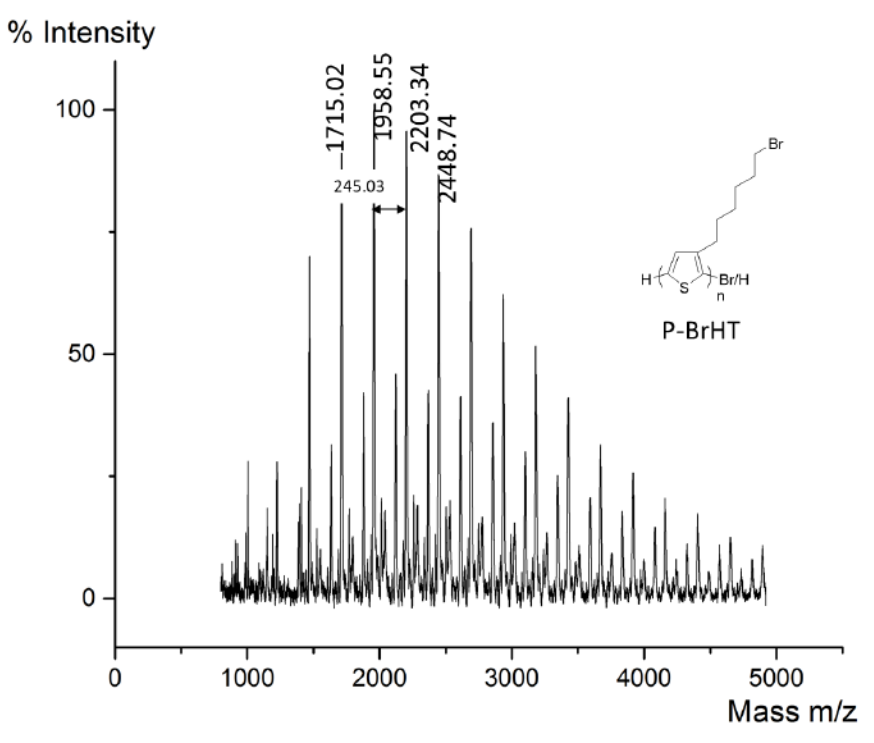


Figure S10. MALDI-TOF mass spectrum of P-BrHT. All MALDI-TOF spectra in this paper cannot reflect the true molecular mass of polymers due to the difficulty for large conjugated polymers to fly and low sensitivity of the machine to large polymers.

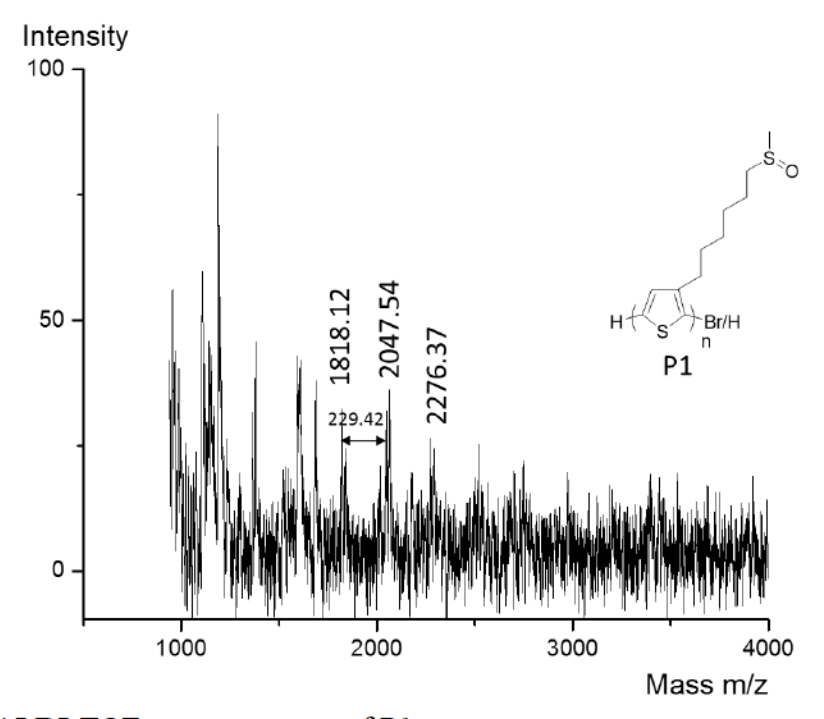


Figure S11. MALDI-TOF mass spectrum of P1.

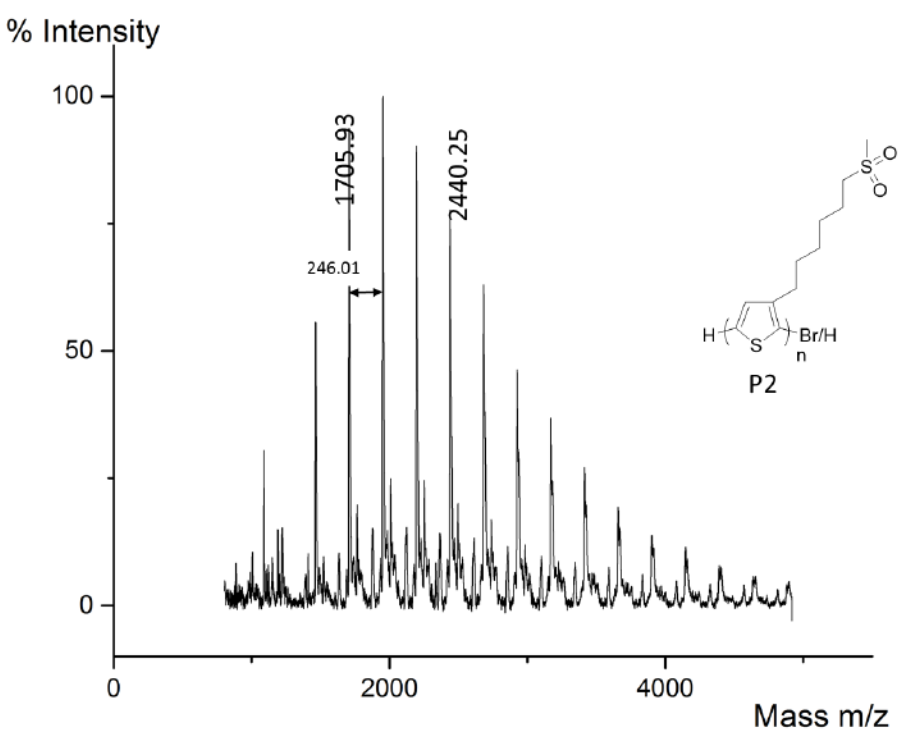


Figure S12. MALDI-TOF mass spectrum of P2.

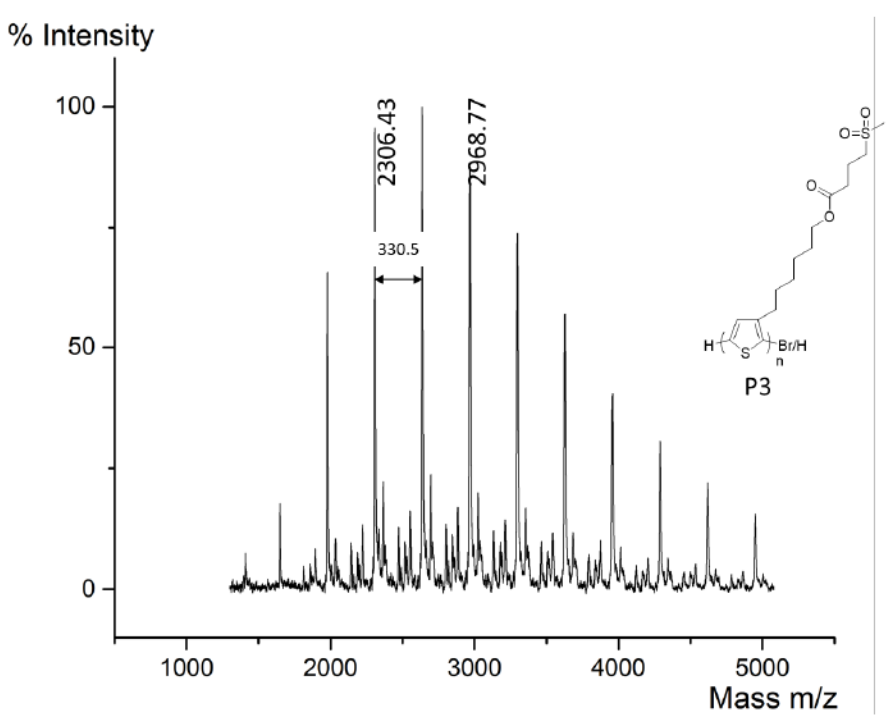


Figure S13. MALDI-TOF mass spectrum of P3.

3. Laser Light Tyndall Effect to Test Polymer Solubility in Solution

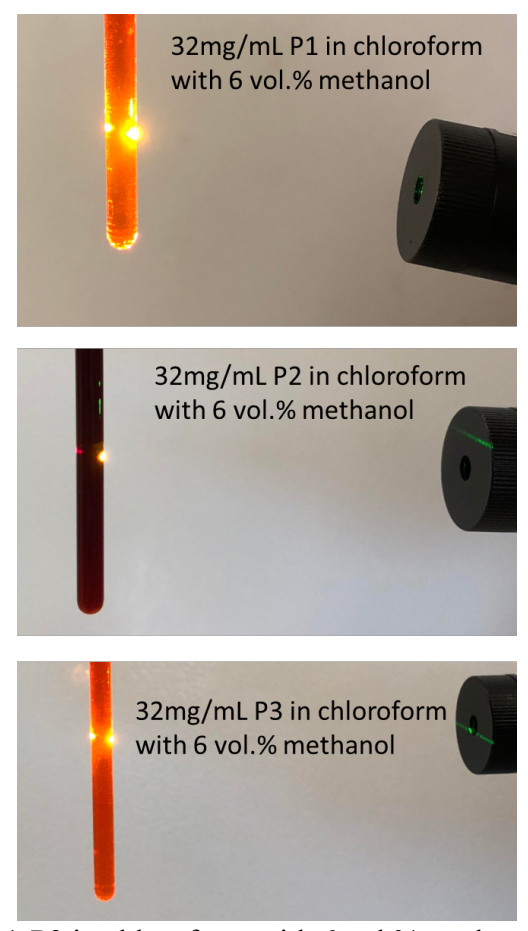


Figure S14. Solubility test of P1-P3 in chloroform with 6 vol.% methanol by using the laser light scattering method. A green laser pointer is used as the laser source. As we can see, no Tyndall effect was seen for all solutions. P1 and P3 show fluorescence, but P2 does not.

4. Normalized UV-Vis Absorption and Fluorescence Spectra for Polymers in Chloroform

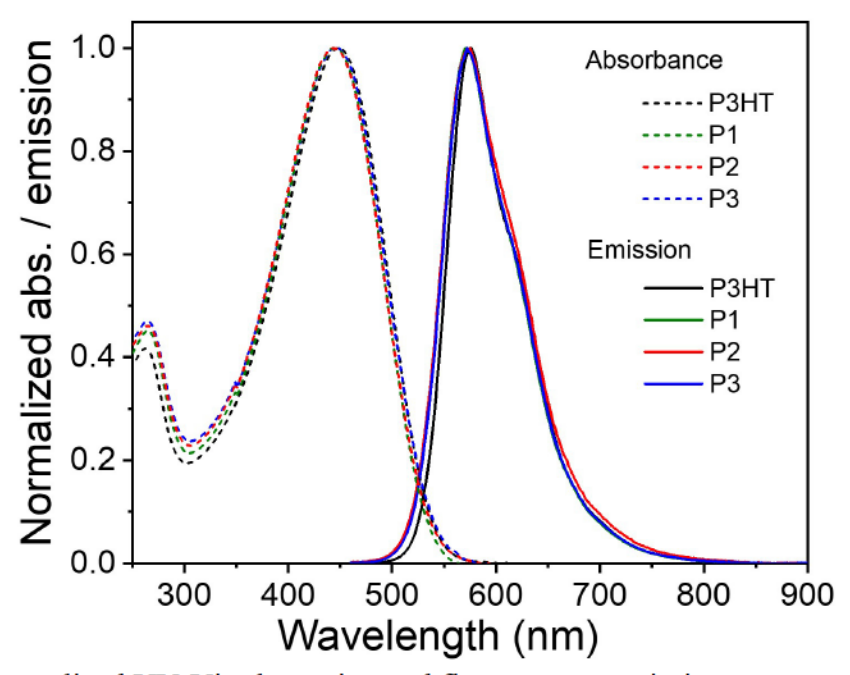


Figure S15. Normalized UV-Vis absorption and fluorescence emission spectra of P3HT, P1, P2, and P3 in chloroform with 6 vol.% methanol.

5. AFM Images of P3HT, P1, P2 and P3 Solution-cast Thin Films

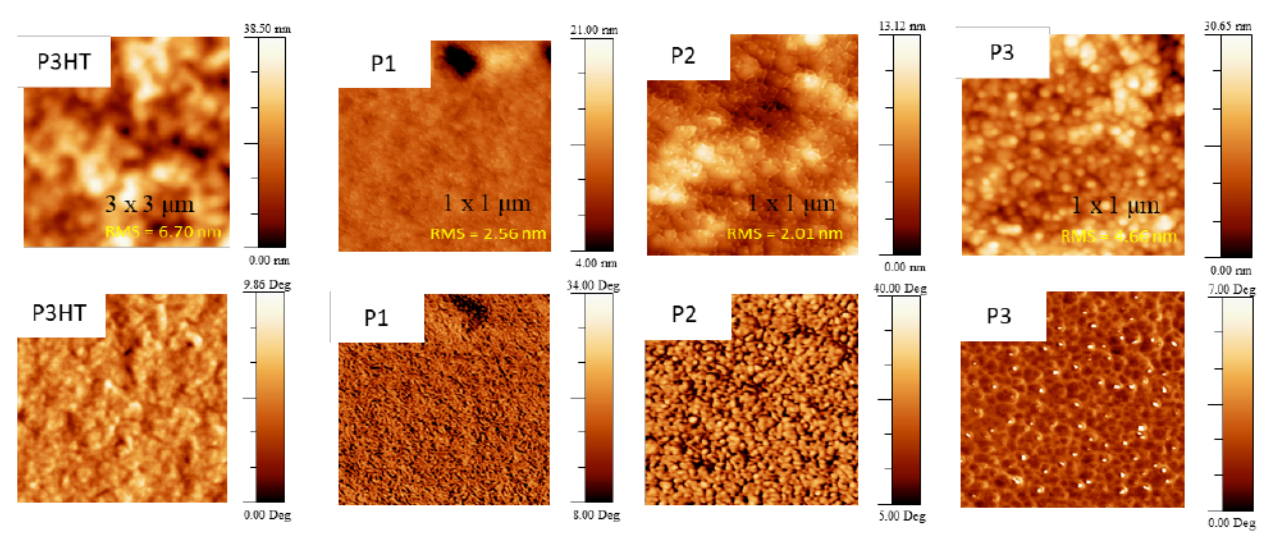


Figure S16. AFM height (top) and phase (bottom) images of annealed films of P3HT, P1, P2 and P3. P3HT film was cast from 10 mg/mL solution in chloroform, and P1, P2 and P3 films were cast from 10 mg/mL solution in chloroform with 6 vol.% methanol (filtered through a 0.45 μm PTFE filter to remove impurity). All films were annealed before AFM measurements: P3HT, P2, and P3 films were annealed at 150 °C for 15 min, and P1 film was annealed at 90 °C for 10 min to avoid possible thermal degradation. From the height images, surface roughnesses were 6.70, 2.56, 2.01, and 4.66 nm for P3HT, P1, P2, and P3, respectively.

6. Fluorescence and UV-Vis Spectra of P3HT/P2 Blends in Thin Films

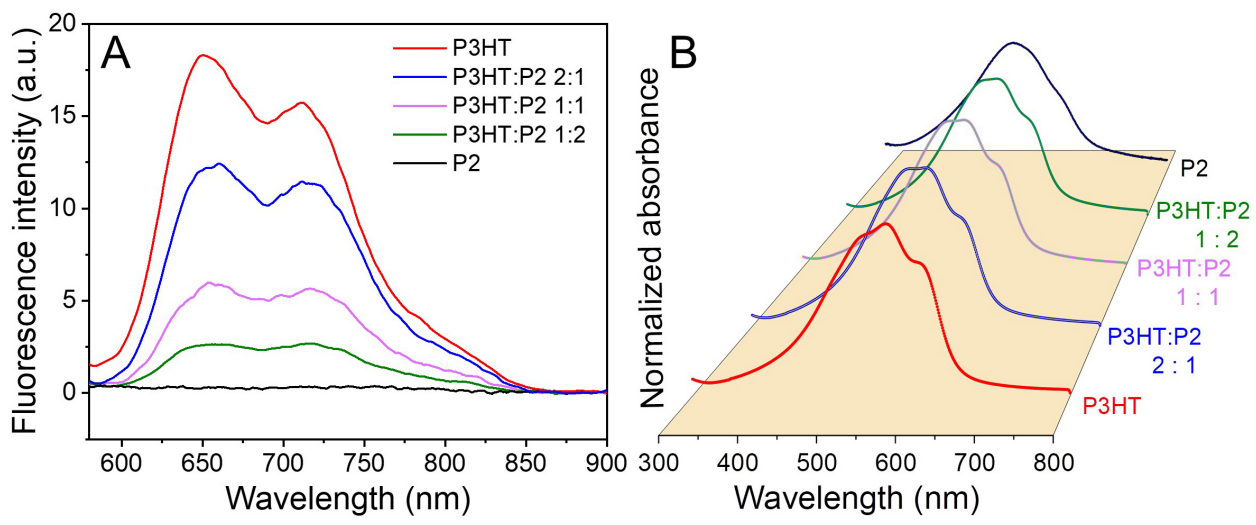


Figure S17. (A) Fluorescence spectra of P3HT and P2 with varied ratios in films and (B) normalized UV-Vis absorption spectra of P3HT and P2 with varied ratios in films. All films were spin-coated from chloroform with 6% of methanol and were annealed at 150 °C for 10 min. Thicknesses of all films were around 65 nm.

7. Cyclic Voltammetry of P2, P3 and R-P3 in DMF

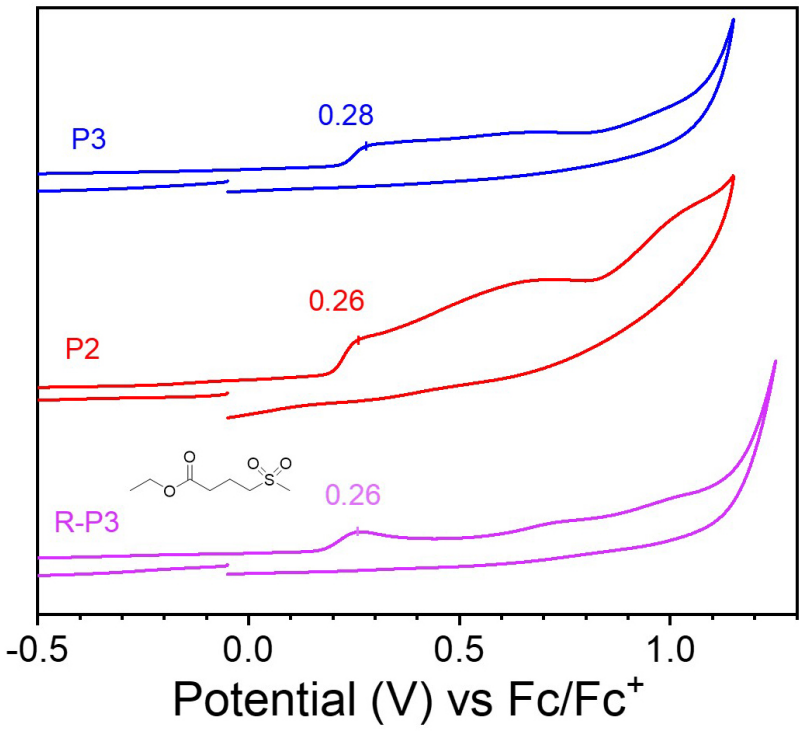


Figure S18. Cyclic voltammetry (CV) curves of P2, P3, and R-P3 in DMF solution (ca. 2 mg/mL).

8. Dielectric Characterization of the P3HT/SiO₂ Bilayer

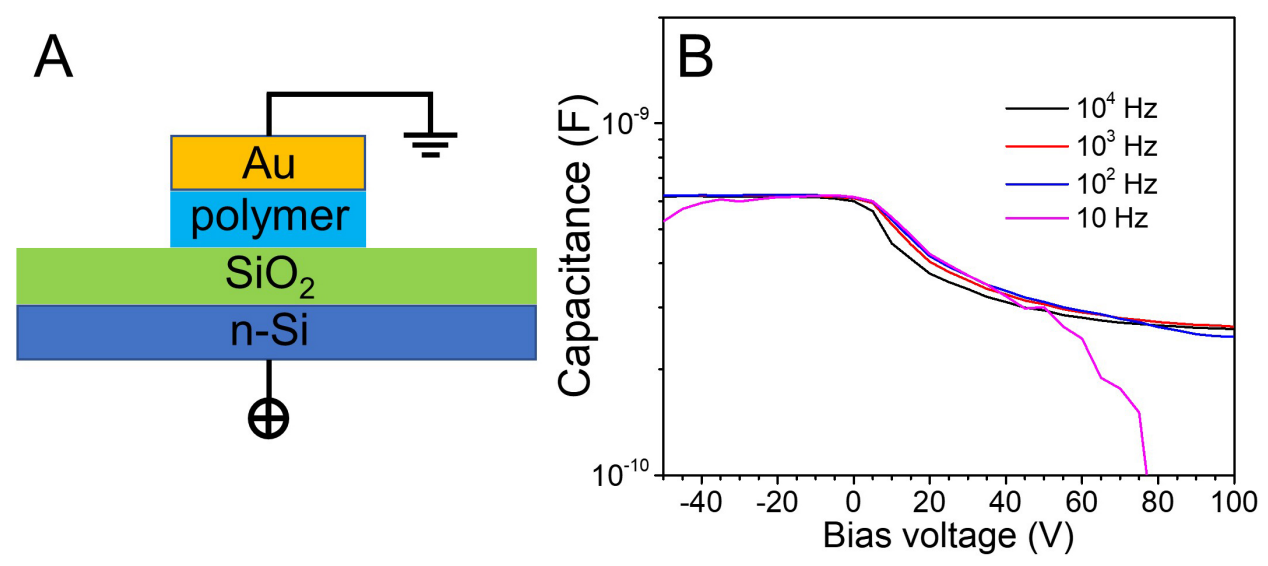


Figure S19. (A) Schematic of the polymer/SiO₂ bilayer capacitor sandwiched between the gold electrode on the top and the n-Si electrode at the bottom. The polymer sample has the same area (4.52 mm²) as the top gold electrode to avoid shorting via pinholes in the SiO₂ layer. On to this bilayer capacitor, a DC bias voltage is applied in addition to the AC measuring voltage of 1 V_{rms} (root-mean square voltage) at various frequencies ranging from 10^4 Hz down to 10 Hz. The positive bias voltage is applied on the n-Si electrode. (B) Measured capacitance as a function of the bias voltage for the P3HT/SiO₂ bilayer capacitor under different frequencies of the measuring AC voltage (1 V_{rms}).

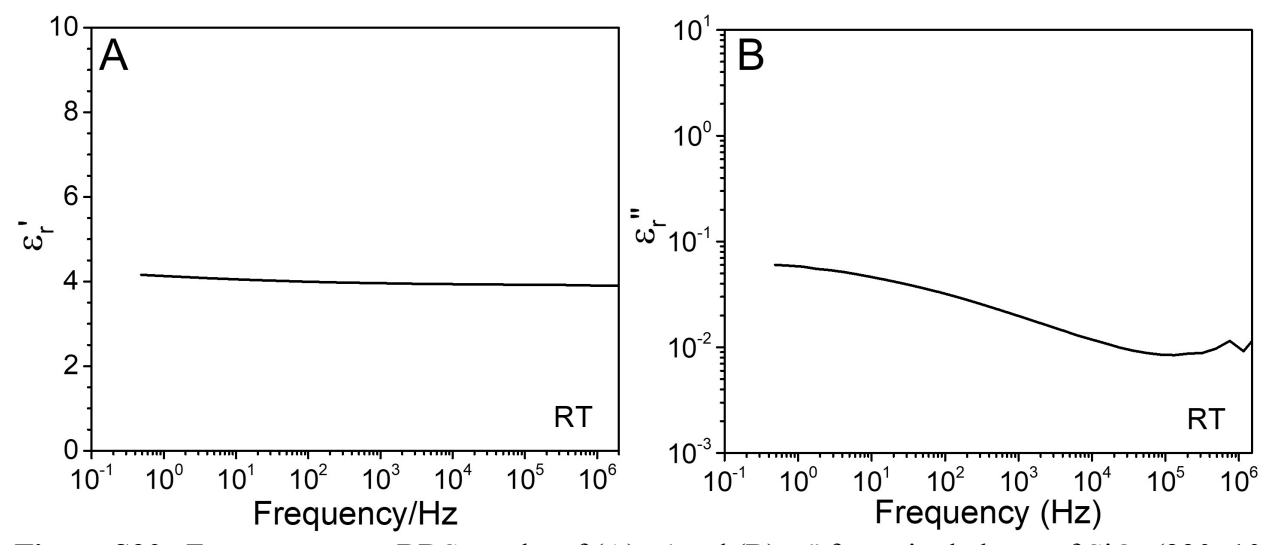


Figure S20. Frequency-scan BDS results of (A) ε_r and (B) ε_r for a single layer of SiO₂ (230±10 nm) sandwiched between the gold and *n*-doped Si electrodes at room temperature.

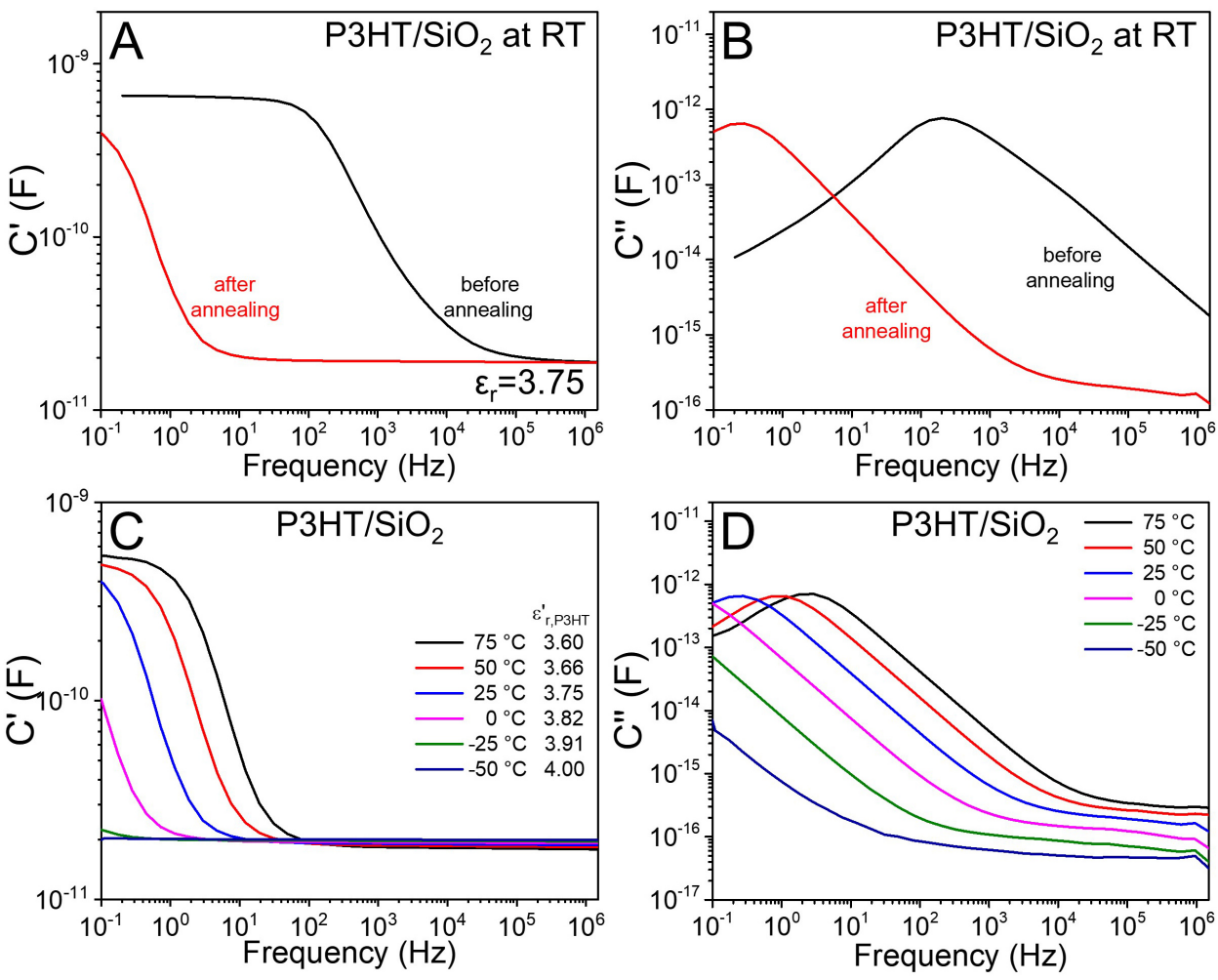


Figure S21. Frequency-scan (A, C) real (C') and (B, D) imaginary (C") parts of the measured capacitance for the P3HT/SiO₂ bilayer capacitor at room temperature. (A, B) Comparison of the C' and C" for the P3HT/SiO₂ bilayer before and after thermal annealing at 75 $^{\circ}$ C in a dry N₂ atmosphere. (C) C' and (D) C" for the N₂-annealed P3HT/SiO₂ bilayer capacitor at different temperatures. The P3HT layer thickness is 6.9 μ m.